RDECOM TR 10-D-107

**U.S. ARMY RESEARCH,
DEVELOPMENT AND
ENGINEERING COMMAND**

TITLE: Design and Experimental Results for the S406 Airfoil

AUTHOR: **Dan M. Somers and Mark D. Maughmer**

COMPANY NAME: **Airfoils, Incorporated**

COMPANY ADDRESS: **122 Rose Drive
Port Matilda PA 16870-7535**

DATE: **August 2010**

FINAL REPORT: **Contract Number W911W6-07-C-0047, SBIR Phase II,
Topic Number A06-006, Proposal Number A2-2972**

Prepared for:

U.S. ARMY RESEARCH, DEVELOPMENT AND ENGINEERING COMMAND, AVIATION APPLIED TECHNOLOGY DIRECTORATE, FORT EUSTIS, VA 23604-5577

AIRFOILS, INCORPORATED
122 ROSE DRIVE
PORT MATILDA, PA 16870-7535 USA
WEBSITE WWW.AIRFOILS.COM
TELEPHONE (814) 357-0500
FACSIMILE (814) 357-0357

DESIGN AND EXPERIMENTAL RESULTS FOR THE S406 AIRFOIL

DAN M. SOMERS
AIRFOILS, INCORPORATED

MARK D. MAUGHMER
THE PENNSYLVANIA STATE UNIVERSITY

AUGUST 2010

ABSTRACT

A 14.25-percent-thick, natural-laminar-flow airfoil, the S406, for rotorcraft applications has been designed and analyzed theoretically and verified experimentally in The Pennsylvania State University Low-Speed, Low-Turbulence Wind Tunnel. The two primary objectives of high maximum lift and low profile drag have been achieved. The constraint on the airfoil thickness has been satisfied, but the one on the pitching moment has not. The airfoil exhibits a docile stall. Comparisons of the theoretical and experimental results generally show good agreement.

INTRODUCTION

Almost all airfoils in use on rotorcraft today were developed under the assumption that extensive laminar flow is not likely on a rotor. (See ref. 1, for example.) For the present application, however, given the relatively low Reynolds numbers and the precision blade manufacturing technique being employed, the achievement of laminar flow warrants exploration.

The airfoil designed under the present effort is intended for the rotor of a small helicopter. To complement the design effort, an investigation was conducted in The Pennsylvania State University Low-Speed, Low-Turbulence Wind Tunnel (ref. 2) to obtain the basic, low-speed, two-dimensional aerodynamic characteristics of the airfoil. The results have been compared with predictions from the method of references 3 and 4 and from the method of reference 5.

SYMBOLS

Values are given in both SI and U.S. Customary Units. Measurements and calculations were made in U.S. Customary Units.

C_p pressure coefficient, $\dfrac{p_l - p_\infty}{q_\infty}$

c airfoil chord, mm (in.)

c_c section chord-force coefficient, $\oint C_p \, d\left(\dfrac{z}{c}\right)$

c_d section profile-drag coefficient, $c_n \sin\alpha + c_c \cos\alpha$ $\int_{\text{Wake}} c_d' \, d\left(\dfrac{h}{c}\right)$, except post stall,

c_d' point drag coefficient (ref. 6)

c_l section lift coefficient, $c_n / \cos\alpha - c_d \tan\alpha$

c_m	section pitching-moment coefficient about quarter-chord point, $-\oint C_p\left(\frac{x}{c}-0.25\right)d\left(\frac{x}{c}\right)+\oint C_p\left(\frac{z}{c}\right)d\left(\frac{z}{c}\right)$
c_n	section normal-force coefficient, $-\oint C_p d\left(\frac{x}{c}\right)$
h	horizontal width in wake profile, mm (in.)
M	free-stream Mach number
p	static pressure, Pa (lbf/ft^2)
q	dynamic pressure, Pa (lbf/ft^2)
R	Reynolds number based on free-stream conditions and airfoil chord
s	arc length along airfoil surface, mm (in.)
t	airfoil thickness, mm (in.)
x	airfoil abscissa, mm (in.)
y	model span station, $y = 0$ at midspan, mm (in.)
z	airfoil ordinate, mm (in.)
α	angle of attack relative to x-axis, deg

Subscripts:

l	local point on airfoil
ll	lower limit of low-drag range
max	maximum
min	minimum
S	separation
T	transition
ul	upper limit of low-drag range
0	zero lift

∞ free-stream conditions

Abbreviations:

L. lower surface

NACA National Advisory Committee for Aeronautics

S. boundary-layer separation location, x_S/c

T. boundary-layer transition location, x_T/c

U. upper surface

AIRFOIL DESIGN

OBJECTIVES AND CONSTRAINTS

The airfoil design specifications are contained in table I. Two primary objectives are evident. The first objective is to achieve a maximum lift coefficient of 1.30 at a Mach number of 0.30 and a Reynolds number of 1.14×10^6. A requirement related to this objective is that the maximum lift coefficient not decrease significantly with transition fixed near the leading edge on both surfaces. In addition, the airfoil should exhibit docile stall characteristics. The second objective is to obtain low profile-drag coefficients from a lift coefficient of 0.20 at a Mach number of 0.59 and a Reynolds number of 2.12×10^6 to a lift coefficient of 0.70 at a Mach number of 0.46 and a Reynolds number of 1.63×10^6.

Two major constraints were placed on the design of the airfoil. First, the zero-lift pitching-moment coefficient must be no more negative than –0.05. Second, the airfoil thickness must equal 14.25-percent chord.

PHILOSOPHY

Given the above objectives and constraints, certain characteristics of the design are apparent. The following sketch illustrates a drag polar that meets the goals for this design.

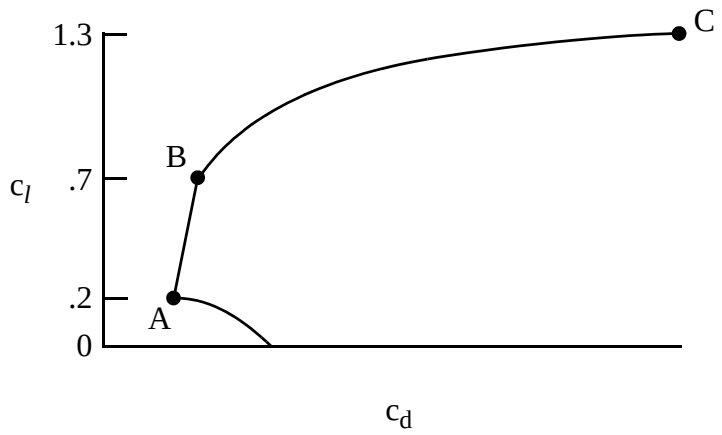

Sketch 1

The desired airfoil shape can be traced to the pressure distributions that occur at the various points in sketch 1. Point A is the lower limit of the low-drag range of lift coefficients; point B, the upper limit. The profile-drag coefficient at point B is not as low as at point A, unlike the polars of many laminar-flow airfoils where the drag coefficient within the laminar bucket is nearly constant. (See, for example, ref. 7.) This characteristic is related to the elimination of significant (drag-producing) laminar separation bubbles on the upper surface for the design range of Reynolds numbers. (See ref. 8.) The drag coefficient increases rapidly outside the low-drag, lift-coefficient range because boundary-layer transition moves quickly toward the leading edge with increasing (or decreasing) lift coefficient. This feature results in a leading edge that produces a suction peak at higher lift coefficients, which ensures that transition on the upper surface will occur very near the leading edge. Thus, the maximum lift coefficient, point C, occurs with turbulent flow along the entire upper surface and, therefore, should be relatively insensitive to roughness at the leading edge.

From the preceding discussion, the pressure distributions along the polar can be deduced. The pressure distribution at point A should look something like sketch 2.

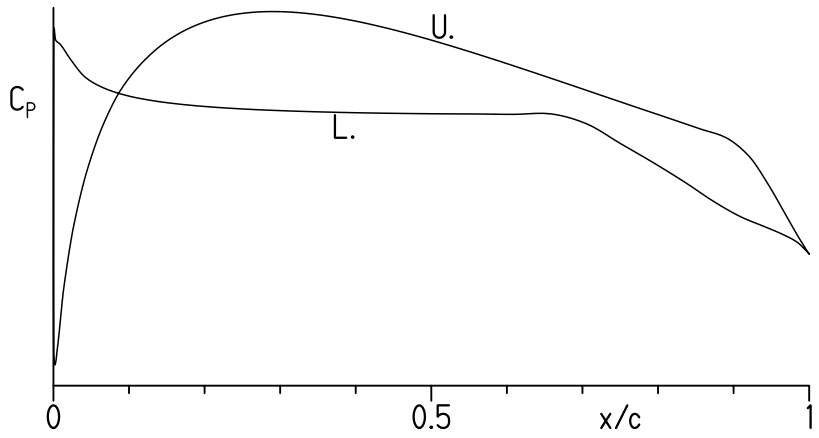

Sketch 2

To achieve low drag, a favorable pressure gradient is desirable along the upper surface to about 30-percent chord. Aft of this point, a short region having a shallow, adverse pressure gradient ("transition ramp") promotes the efficient transition from laminar to turbulent flow (ref. 9). The transition ramp is followed by a slightly convex pressure recovery. The specific pressure recovery employed represents a compromise between maximum lift, drag, pitching moment, stall characteristics, and drag divergence. The steep, adverse pressure gradient aft of about 90-percent chord is a "separation ramp," originally proposed by F. X. Wortmann,[1] which confines turbulent separation to a small region near the trailing edge. By constraining the movement of the separation point at high angles of attack, higher lift coefficients can be achieved with little drag penalty. This feature has the added benefit of promoting docile stall characteristics. (See ref. 10.)

Along the lower surface, the pressure gradient is initially adverse and then approximately zero to about 65-percent chord. Thus, transition is imminent over the entire forward portion of the lower surface. (See ref. 11.) This concept allows a wide low-drag range to be achieved and increases the loading in the leading-edge region. The forward loading serves to balance, with respect to the pitching-moment constraint, the aft loading, both of which contribute to the achievement of the specified maximum lift coefficient and low profile-drag coefficients. This region is followed by a transition ramp and then a roughly linear pressure recovery. The pressure recovery must begin farther forward than optimum for low drag and the constrained pitching moment to alleviate separation at lower lift coefficients, especially with transition fixed near the leading edge.

[1]Director, Institute for Aerodynamics and Gas Dynamics, University of Stuttgart, Germany, 1974–1985.

The amounts of pressure recovery on the upper and lower surfaces are determined by the airfoil-thickness and pitching-moment constraints.

At point B, the pressure distribution should look like sketch 3.

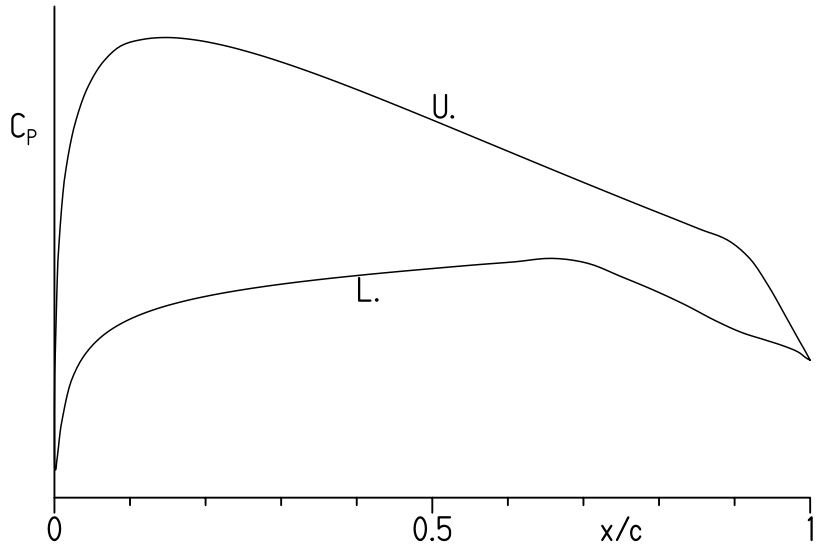

Sketch 3

No suction peak exists at the leading edge. Instead, a rounded peak occurs aft of the leading edge, which allows some laminar flow although not to the extent of point A.

EXECUTION

Given the pressure distributions previously discussed, the design of the airfoil is reduced to the inverse problem of transforming the pressure distributions into an airfoil shape. The Eppler Airfoil Design and Analysis Code (refs. 3 and 4) was used because of its unique capability for multipoint design and because of confidence gained during the design, analysis, and experimental verification of many other airfoils. (See ref. 12, for example.)

The airfoil is designated the S406. The airfoil shape and coordinates are available from Airfoils, Incorporated. The airfoil thickness is 14.25-percent chord, which satisfies the design constraint.

THEORETICAL PROCEDURE

The theoretical results are predicted using the method of references 3 and 4 (PROFIL07), commonly known as the Eppler code, and the method of reference 5 (MSES 3.0). Critical amplification factors of 11 and 9 were specified for the computations using the method of references 3 and 4 and the method of reference 5, respectively. Because the maximum lift coefficient computed by the method of references 3 and 4 is not always realistic, an empirical criterion has been applied to the computed results. The criterion assumes the maximum lift coefficient has been reached if the drag coefficient of the upper surface reaches a certain value that is a function of the Reynolds number and the wind-tunnel facility.

Because the free-stream Mach number for all wind-tunnel test conditions did not exceed 0.2, the flow can be considered incompressible for the purpose of comparing the theoretical and experimental results. This allows the (incompressible) conformal-mapping (design) method of references 3 and 4 and the fast, subcritical flow solver of reference 5 to be used.

EXPERIMENTAL PROCEDURE

WIND TUNNEL

The Pennsylvania State University Low-Speed, Low-Turbulence Wind Tunnel (ref. 2) is a closed-throat, single-return, atmospheric tunnel (fig. 1). The test section is 101.3 cm (39.9 in.) high by 147.6 cm (58.1 in.) wide (fig. 2). Electrically actuated turntables provide positioning and attachment for the two-dimensional model. The turntables are flush with the top and bottom tunnel walls and rotate with the model. The axis of rotation coincided approximately with the midchord of the model, which was mounted vertically between the turntables. The gaps between the model and the turntables were sealed. The turbulence intensity in the test section is approximately 0.05 percent at 46 m/s (150 ft/s).

MODEL

The aluminum, wind-tunnel model was fabricated by Advanced Technologies, Incorporated, Newport News, Virginia, using a numerically controlled milling machine. The model had a chord of 457.04 mm (17.994 in.) and a span of 107.95 cm (42.50 in.) and, thus, extended through both turntables. Upper- and lower-surface orifices were located to one side of midspan at the staggered positions listed in table II. All the orifices were 0.51 mm (0.020 in.) in diameter, except the trailing-edge orifice, which was 0.25 mm (0.010 in.) in diameter, with their axes perpendicular to the surface. The surfaces of the model were sanded to ensure an aerodynamically smooth finish. The measured model contour was within 0.13 mm (0.005 in.) of the prescribed shape.

WAKE-SURVEY PROBE

A total- and static-pressure, wake-survey probe (fig. 3) was mounted from the top tunnel wall (fig. 2). The probe was positioned 53 cm (21 in.) from the top wall (i.e., about midspan) and automatically aligned with the wake-centerline streamline. A traverse mechanism incrementally positioned the probe to survey the wake. The increment was 1.27 mm (0.050 in.) for traverses less than 254.0 mm (10.00 in.) and 2.54 mm (0.100 in.) for longer traverses, which were occasionally required near the maximum angle of attack. The tip of the probe was located 0.83 chord downstream of the trailing edge of the model.

INSTRUMENTATION

Basic tunnel pressures and the wake pressures were measured with precision transducers. Measurements of the pressures on the model were made by an automatic pressure-scanning system utilizing precision transducers. Data were obtained and recorded by an electronic data-acquisition system.

METHODS

The pressures measured on the model were reduced to standard pressure coefficients and numerically integrated to obtain section normal-force and chord-force coefficients and section pitching-moment coefficients about the quarter-chord point. Section profile-drag coefficients were computed from the wake total and static pressures by the method of reference 6. Wake surveys were not performed, however, at most post-stall angles of attack, in which case, the profile-drag coefficients were computed from the normal- and chord-force coefficients.

Standard, low-speed, wind-tunnel boundary corrections (ref. 13) have been applied to the data. It should be noted, however, that the pressure distributions themselves are uncorrected. The wake-survey-probe total-pressure-tube displacement correction (ref. 6) has been taken into account.

TESTS

The model was tested at Reynolds numbers based on airfoil chord of 0.5×10^6, 0.7×10^6, 1.0×10^6, and 1.5×10^6 with transition free (smooth) and with transition fixed by roughness at 2-percent chord on the upper surface and 7-percent chord on the lower surface. The grit roughness was sized using the method of reference 14 and sparsely distributed along 3-mm (0.1-in.) wide strips applied to the model with lacquer. (See table III(a).) The model was also tested with a roughness equivalent to NACA standard roughness (ref. 7), which consisted of grit roughness having a nominal size of 0.211 mm (0.0083 in.) applied to the model with lacquer and sparsely distributed from the leading edge to an arc length of 8-percent chord on the upper and lower surfaces. (See table III(b).) (The grit size was scaled from the NACA

standard-roughness grit size by the ratio of the model chords used in the two wind tunnels: 457.04 mm (17.994 in.) in the present investigation and 609.6 mm (24.00 in.) in the NACA tests.) The Mach number did not exceed 0.2 for any test condition.

It should be noted that the test Mach numbers are much lower than the operational values of the intended application.

Starting from 0°, the angle of attack was increased to post-stall values. The angle of attack was then decreased from 0° to below that for zero lift.

DISCUSSION OF RESULTS

THEORETICAL RESULTS

Pressure Distributions

The inviscid pressure distributions at various angles of attack and Mach numbers predicted using the method of references 3 and 4 are shown in figure 4.

Section Characteristics

The section characteristics at the three design conditions with transition free and fixed are shown in figures 5 through 7. Based on the predictions, all the design objectives and constraints have been met, except for the zero-lift pitching-moment coefficient, which exceeds the constraint.

EXPERIMENTAL RESULTS

Pressure Distributions

The pressure distributions at various angles of attack for a Reynolds number of 1.00×10^6 and a Mach number of 0.11 with transition free are shown in figure 8. At an angle of attack of –4.05° (fig. 8(a)), transition probably occurs around 75-percent chord on the upper surface and near the leading edge on the lower surface. At an angle of attack of –2.02° (fig. 8(a)), which corresponds to the lower limit of the low-drag, lift-coefficient range, a short laminar separation bubble is evident on the lower surface around 75-percent chord. As the angle of attack is increased, a short laminar separation bubble becomes more evident on the upper surface and moves forward whereas the bubble on the lower surface moves slowly aft (figs. 8(a)–8(c)). At an angle of attack of 9.17° (fig. 8(c)), turbulent, trailing-edge separation occurs on the upper surface. The amount of separation increases with increasing angle of attack (figs. 8(c) and 8(d)). The maximum lift coefficient occurs at an angle of attack of 13.20° (fig. 8(d)). As the angle of attack is increased further, the separation point continues to move forward, although the leading-edge pressure peak does not fall (fig. 8(e)).

Section Characteristics

The section characteristics with transition free, transition fixed, and scaled, NACA standard roughness, denoted "rough," are shown in figure 9 and tabulated in the appendix. For a Reynolds number of 1.00×10^6 and a Mach number of 0.11 with transition free (fig. 9(c)), the maximum lift coefficient is 1.25. For a Reynolds number of 1.50×10^6 and a Mach number of 0.17 with transition free (fig. 9(d)), the zero-lift pitching-moment coefficient is −0.066, the lower limit of the low-drag range of lift coefficients is about 0.15, and the maximum lift-to-drag ratio occurs at a lift coefficient of about 0.86. (Because the upper limit of the low-drag range is not sharply defined, a precise value for the upper limit cannot be given.)

The effects of Reynolds number on the section characteristics are summarized in figure 10. In general, with transition free, the lift-curve slope, the maximum lift coefficient, the lower limit of the low-drag range, and the magnitude of the pitching-moment coefficients increase with increasing Reynolds number. The zero-lift angle of attack and the zero-lift pitching-moment coefficient are relatively unaffected by Reynolds number. The profile-drag coefficients generally decrease with increasing Reynolds number. The airfoil exhibits docile stall characteristics that become less docile with increasing Reynolds number.

The effect of fixing transition on the section characteristics is shown in figure 9. In general, the lift-curve slope, the maximum lift coefficient, and the magnitude of the pitching-moment coefficients decrease with transition fixed. These results are primarily a consequence of the boundary-layer displacement effect, which decambers the airfoil because the displacement thickness is greater with transition fixed than with transition free. In addition, the maximum lift coefficient decreases with transition fixed because the roughness induces earlier trailing-edge separation. The reduction in maximum lift coefficient is small, averaging 4 percent over the test Reynolds number range. The zero-lift angle of attack and the zero-lift pitching-moment coefficient are relatively unaffected by fixing transition.

It should be noted that, for most test conditions, the Reynolds number based on local velocity and boundary-layer displacement thickness at the roughness location is too low to support turbulent flow. (See ref. 15.) Accordingly, to force transition, the roughness must be so large that it increases the displacement thickness, which abnormally decreases the lift coefficient and the magnitude of the pitching-moment coefficient and increases the drag coefficient. Conversely, at low lift coefficients, the roughness on the upper surface, which is sized for higher lift coefficients, is too small to force transition, resulting in incorrectly low drag coefficients.

The effect of the scaled, NACA standard roughness on the section characteristics is shown in figure 9. The effect is more severe than that of fixing transition. The reduction in maximum lift coefficient is much larger, averaging 18 percent for Reynolds numbers greater than 0.5×10^6. For a Reynolds number of 0.5×10^6, the height of the scaled, NACA standard roughness is less than the critical height computed using the method of reference 14. (See table III.) Accordingly, the effects of this roughness for a Reynolds number of 0.50×10^6 are inconsistent (fig. 9(a)). It should be remembered that the effect of roughness is proportional to the ratio of the roughness height to the boundary-layer thickness. Because the height of the

scaled, NACA standard roughness and the airfoil chord are constant, the effect of this roughness typically increases with increasing Reynolds number (because increasing Reynolds number results in decreasing boundary-layer thickness).

The variations of maximum lift coefficient and minimum profile-drag coefficient with Reynolds number are shown in figures 11 and 12, respectively. With transition free, the maximum lift coefficient increases with increasing Reynolds number whereas the minimum profile-drag coefficient decreases, which are typical trends for most airfoils. (The maximum lift coefficient and minimum drag coefficient for a Reynolds number of 0.50×10^6 with scaled roughness are too high and too low, respectively, probably because the roughness is too small to force transition immediately, as previously discussed.)

COMPARISON OF THEORETICAL AND EXPERIMENTAL RESULTS

Pressure Distributions

The comparison of the theoretical and experimental pressure distributions at various angles of attack is shown in figure 13. It should be noted that the pressure distributions predicted using the method of references 3 and 4 (PROFIL07) are inviscid and incompressible, whereas the pressure distributions predicted using the method of reference 5 (MSES 3.0) as well as the experimental pressure distributions were obtained for a Reynolds number of 1.00×10^6 and a Mach number of 0.11 with transition free. It should also be noted that the theoretical lift coefficient from the method of references 3 and 4 is calculated from the lift-curve slope and the angle of attack relative to the zero-lift line, whereas the lift coefficient from the method of reference 5 and from the experiment is derived from the integrated pressure distribution. (See refs. 3–6.) Thus, at a given lift coefficient, the pressure distribution predicted using the method of references 3 and 4 does not necessarily have the same area as the measured pressure distribution. It should be noticed that the angle of attack shown in figure 13 is the theoretical value from the method of references 3 and 4, not the experimental value. Also, the lift coefficient shown in this figure only is the uncorrected value.

With respect to the method of references 3 and 4, at a lift coefficient of 0.13 (fig. 13(a)), which corresponds to the lower limit of the low-drag range, the pressure coefficients and the pressure gradients agree well, except where laminar separation bubbles are present and near the trailing edge. The latter disparity is probably the result of the boundary-layer displacement effect. At a lift coefficient of 0.67 (fig. 13(b)), although the pressure coefficients do not match exactly, the pressure gradients agree reasonably well, again except where bubbles are present and near the trailing edge. At the experimental maximum lift coefficient (fig. 13(c)), the agreement is poor because the effect of the upper-surface, trailing-edge separation on the pressure distribution is not modelled in the method of references 3 and 4.

With respect to the method of reference 5, at a lift coefficient of 0.13 (fig. 13(a)), the pressure coefficients and the pressure gradients agree remarkably well. The location of the lower-surface laminar separation bubble is predicted well, but that of the upper-surface bubble is aft of the measured location. At a lift coefficient of 0.67 (fig. 13(b)), although the pressure

coefficients do not match exactly, the pressure gradients agree well. The predicted location of the upper-surface bubble is again aft of the measured location. At the experimental maximum lift coefficient (fig. 13(c)), the agreement is poor because the extensive, upper-surface, trailing-edge separation is not predicted by the method of reference 5.

Section Characteristics

The comparison of the theoretical and experimental section characteristics with transition free is shown in figure 14. The maximum lift coefficient estimated using the previously discussed empirical criterion applied to the predictions from the method of references 3 and 4 (PROFIL07) agrees well with the measurements. The method of reference 5 (MSES 3.0) significantly overpredicts the maximum lift coefficient. The method of references 3 and 4 generally overpredicts the profile-drag coefficients and the magnitude of the pitching-moment coefficients, although the agreement improves with increasing Reynolds number. The method of reference 5 generally underpredicts the drag coefficients and overpredicts the magnitude of the pitching-moment coefficients and the agreement worsens with increasing Reynolds number. Both methods predict the zero-lift angle of attack and the zero-lift pitching-moment coefficient, the lower limit of the low-drag range, and the lift-curve slope reasonably well, although both underpredict the effect of the trailing-edge separation on the lift coefficient at higher angles of attack.

The comparison of the theoretical and experimental section characteristics with transition fixed is shown in figure 15. In general, the predicted characteristics show similar tendencies as with transition free, although the general agreement is poorer, particularly with respect to the drag coefficients, probably because of the abnormalities introduced by the roughness, as discussed previously.

CONCLUDING REMARKS

A 14.25-percent-thick, natural-laminar-flow airfoil, the S406, intended for rotorcraft applications has been designed and analyzed theoretically and verified experimentally in The Pennsylvania State University Low-Speed, Low-Turbulence Wind Tunnel. The two primary objectives of a high maximum lift coefficient and low profile-drag coefficients have been achieved. The constraint on the airfoil thickness has been satisfied, but the one on the zero-lift pitching-moment coefficient has not. The airfoil exhibits a docile stall. Comparisons of the theoretical and experimental results generally show good agreement.

ACKNOWLEDGMENTS

This effort was sponsored by the U.S. Army. Preston B. Martin served as the technical monitor.

REFERENCES

1. Noonan, Kevin W.: Aerodynamic Characteristics of Two Rotorcraft Airfoils Designed for Application to the Inboard Region of a Main Rotor Blade. NASA TP-3009, 1990.

2. Brophy, Christopher M.: Turbulence Management and Flow Qualification of The Pennsylvania State University Low Turbulence, Low Speed, Closed Circuit Wind Tunnel. M. S. Thesis, Pennsylvania State Univ., 1993.

3. Eppler, Richard: Airfoil Design and Data. Springer-Verlag (Berlin), 1990.

4. Eppler, Richard: Airfoil Program System "PROFIL07." User's Guide. Richard Eppler, c.2007.

5. Drela, M.: Design and Optimization Method for Multi-Element Airfoils. AIAA Paper 93-0969, Feb. 1993.

6. Pankhurst, R. C.; and Holder, D. W.: Wind-Tunnel Technique. Sir Isaac Pitman & Sons, Ltd. (London), 1965.

7. Abbott, Ira H.; Von Doenhoff, Albert E.; and Stivers, Louis S., Jr.: Summary of Airfoil Data. NACA Rep. 824, 1945. (Supersedes NACA WR L-560.)

8. Eppler, Richard; and Somers, Dan M.: Airfoil Design for Reynolds Numbers Between 50,000 and 500,000. Proceedings of the Conference on Low Reynolds Number Airfoil Aerodynamics, UNDAS-CP-77B123, Univ. of Notre Dame, June 1985, pp. 1–14.

9. Wortmann, F. X.: Experimental Investigations on New Laminar Profiles for Gliders and Helicopters. TIL/T.4906, British Minist. Aviat., Mar. 1960. (Translated from Z. Flugwissenschaften, Bd. 5, Heft 8, Aug. 1957, S. 228–243.)

10. Maughmer, Mark D.; and Somers, Dan M.: Design and Experimental Results for a High-Altitude, Long-Endurance Airfoil. J. Aircr., vol. 26, no. 2, Feb. 1989, pp. 148–153.

11. Eppler, R.: Laminar Airfoils for Reynolds Numbers Greater Than 4×10^6. B-819-35, Apr. 1969. (Available from NTIS as N69-28178; translated from Ingenieur-Archiv, Bd. 38, Heft 4/5, 1969, S. 232–240.)

12. Somers, Dan M.: Subsonic Natural-Laminar-Flow Airfoils. Natural Laminar Flow and Laminar Flow Control, R. W. Barnwell and M. Y. Hussaini, eds., Springer-Verlag New York, Inc., 1992, pp. 143–176.

13. Allen, H. Julian; and Vincenti, Walter G.: Wall Interference in a Two-Dimensional-Flow Wind Tunnel, With Consideration of the Effect of Compressibility. NACA Rep. 782, 1944. (Supersedes NACA WR A-63.)

14. Braslow, Albert L.; and Knox, Eugene C.: Simplified Method for Determination of Critical Height of Distributed Roughness Particles for Boundary-Layer Transition at Mach Numbers From 0 to 5. NACA TN 4363, 1958.

15. Schubauer, G. B.; and Klebanoff, P. S.: Contributions on the Mechanics of Boundary-Layer Transition. NACA Rep. 1289, 1956.

TABLE I.- AIRFOIL DESIGN SPECIFICATIONS

Parameter	Objective/ Constraint	Mach Number M	Reynolds Number R	Priority
Minimum lift coefficient $c_{l,\min}$	0.10	0.59	2.12×10^6	Low
Maximum lift coefficient $c_{l,\max}$	1.30	0.30	1.14×10^6	High
Lower limit of low-drag, lift-coefficient range $c_{l,\mathrm{ll}}$	0.20	0.59	2.12×10^6	Medium
Upper limit of low-drag, lift-coefficient range $c_{l,\mathrm{ul}}$	0.70	0.46	1.63×10^6	High
Zero-lift pitching-moment coefficient $c_{m,0}$	≥ -0.05	0.59	2.12×10^6	Low
Thickness t/c	0.1425			High
Other requirements: Natural-laminar-flow airfoil Maximum lift coefficient $c_{l,\max}$ independent of leading-edge roughness Docile stall characteristics				

TABLE II.- MODEL ORIFICE LOCATIONS

[c = 457.04 mm (17.994 in.)]

Upper Surface		Lower Surface	
x/c	y, mm (in.)	x/c	y, mm (in.)
0.00000	−139.96 (−5.510)	0.00079	−153.15 (−6.029)
.00031	−138.95 (−5.470)	.00848	−152.14 (−5.990)
.00440	−137.93 (−5.430)	.02202	−150.86 (−5.939)
.01257	−136.92 (−5.390)	.04143	−149.08 (−5.869)
.02566	−135.64 (−5.340)	.06613	−147.06 (−5.790)
.04235	−134.12 (−5.280)	.09573	−144.52 (−5.690)
.06311	−132.34 (−5.210)	.12987	−141.72 (−5.580)
.08804	−130.32 (−5.131)	.16813	−138.42 (−5.450)
.11600	−128.02 (−5.040)	.21003	−134.87 (−5.310)
.14785	−125.24 (−4.931)	.25499	−131.06 (−5.160)
.18296	−122.18 (−4.810)	.30266	−126.99 (−5.000)
.22104	−118.88 (−4.680)	.35222	−122.93 (−4.840)
.26184	−115.58 (−4.550)	.40325	−118.61 (−4.670)
.30481	−112.02 (−4.410)	.45511	−114.29 (−4.500)
.34998	−108.21 (−4.260)	.50723	−109.97 (−4.329)
.39684	−104.41 (−4.110)	.55889	−105.65 (−4.159)
.44477	−100.34 (−3.950)	.60956	−101.32 (−3.989)
.49359	−96.28 (−3.790)	.65862	−97.27 (−3.830)
.54278	−92.20 (−3.630)	.70553	−93.46 (−3.680)
.59187	−88.15 (−3.471)	.75096	−89.65 (−3.530)
.64040	−84.08 (−3.310)	.79465	−86.09 (−3.389)
.68785	−80.02 (−3.150)	.83616	−82.54 (−3.250)
.73377	−76.21 (−3.000)	.87461	−79.23 (−3.119)
.77756	−81.54 (−3.210)	.91038	−76.18 (−2.999)
.81914	−86.39 (−3.401)	.94209	−87.36 (−3.439)
.85703	−90.96 (−3.581)	.96727	−96.26 (−3.790)
.89108	−95.00 (−3.740)	.98558	−102.59 (−4.039)
.92369	−98.99 (−3.897)	.99683	−106.28 (−4.184)
.95101	−102.29 (−4.027)	1.00000	−109.20 (−4.299)
.97255	−104.83 (−4.127)		
.98815	−106.61 (−4.197)		
.99681	−107.88 (−4.247)		

TABLE III.- ROUGHNESS LOCATIONS AND SIZES

(a) Transition fixed

R	Upper surface			Lower surface		
	x/c	Grit number	Nominal size, mm (in.)	x/c	Grit number	Nominal size, mm (in.)
0.5×10^6	0.02	60	0.297 (0.0117)	0.07	30	0.711 (0.0280)
0.7×10^6		80	0.211 (0.0083)		36	0.589 (0.0232)
1.0×10^6		100	0.150 (0.0059)		54	0.351 (0.0138)
1.5×10^6		120	0.124 (0.0049)		70	0.249 (0.0098)

(b) Scaled, NACA standard roughness

R	Upper surface			Lower surface		
	s/c	Grit number	Nominal size, mm (in.)	s/c	Grit number	Nominal size, mm (in.)
0.5×10^6	0 to 0.08	80	0.211 (0.0083)	0 to 0.08	80	0.211 (0.0083)
0.7×10^6						
1.0×10^6						
1.5×10^6						

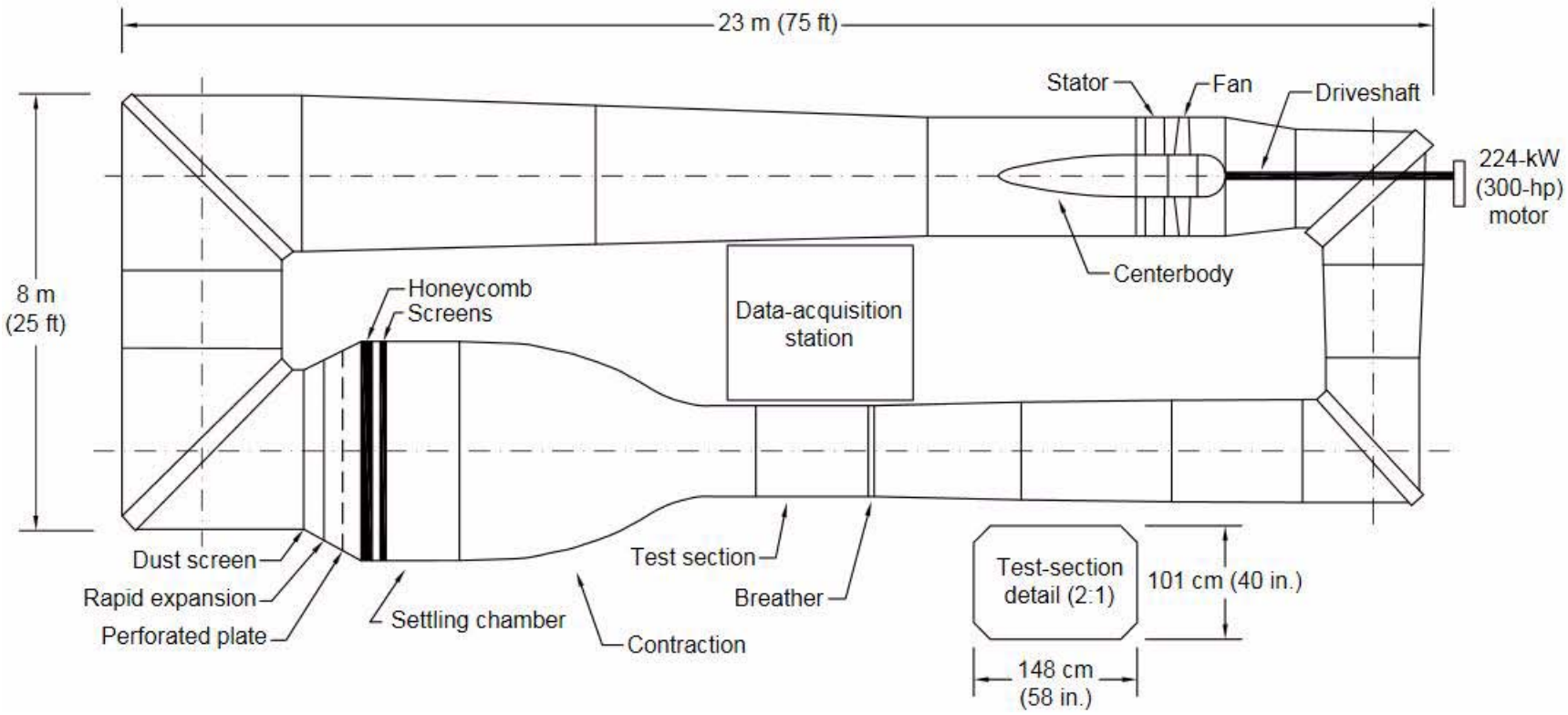

Figure 1.- The Pennsylvania State University Low-Speed, Low-Turbulence Wind Tunnel.

Figure 2.- Typical airfoil model and wake-survey probe mounted in test section.

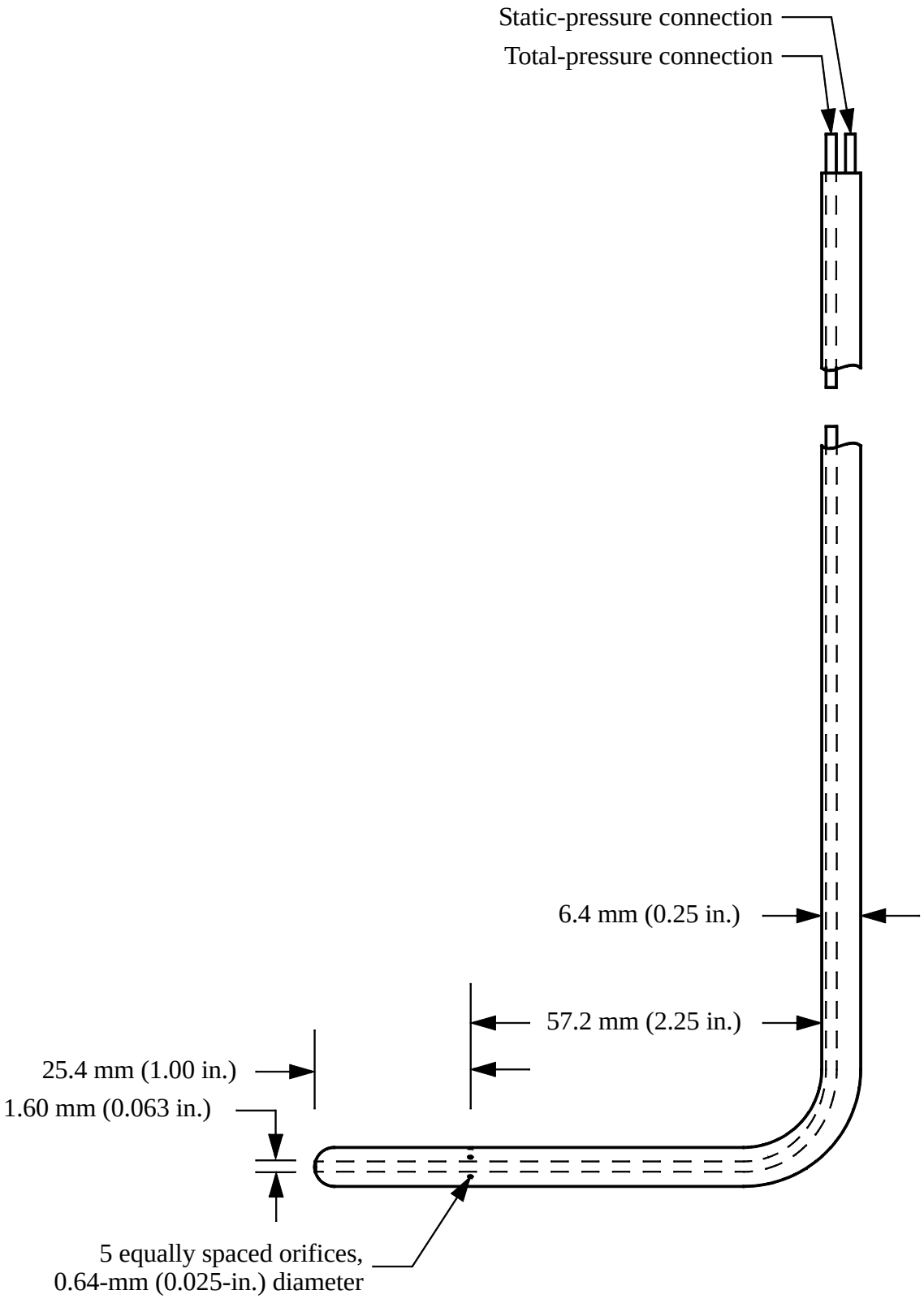

Figure 3.- Wake-survey probe.

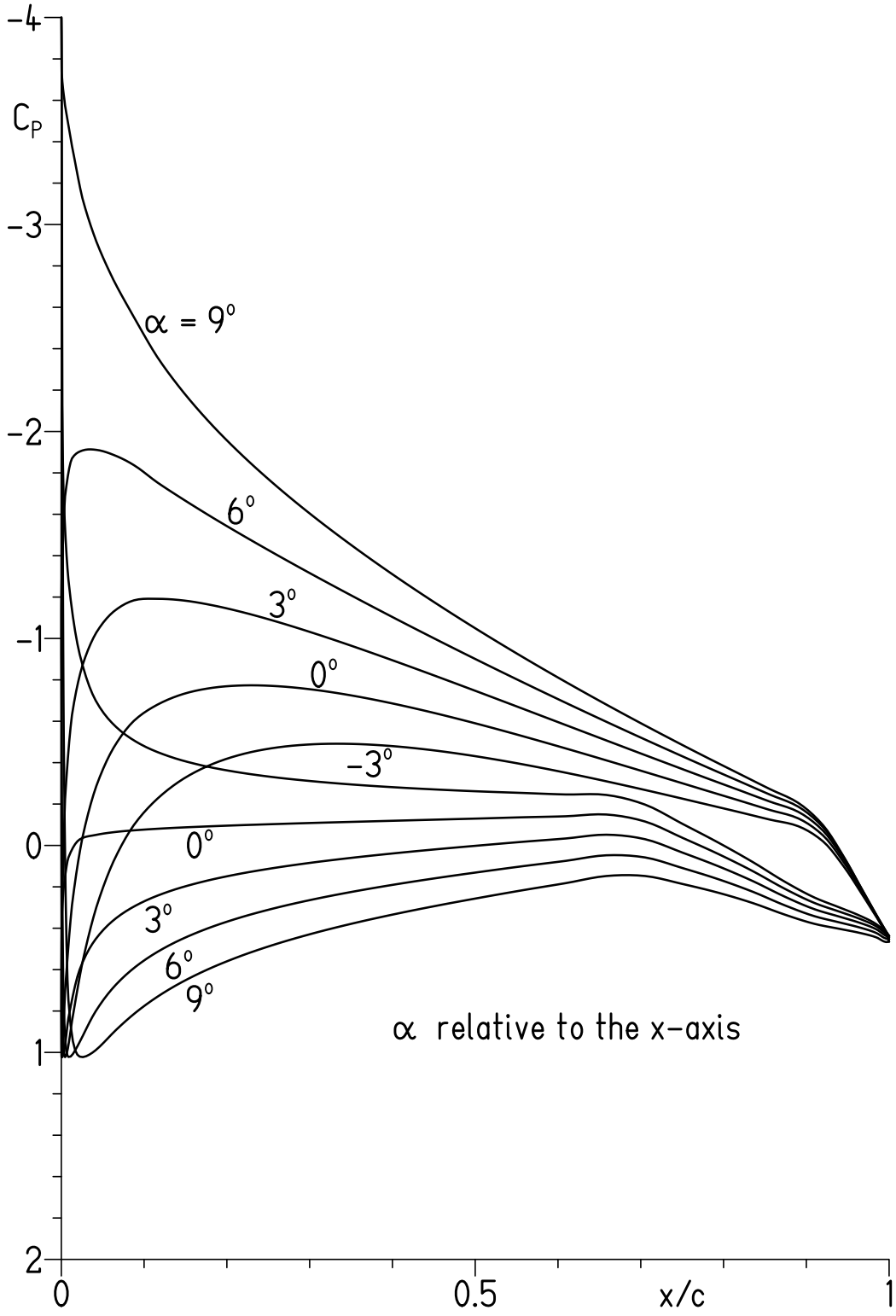

(a) M = 0.30.

Figure 4.- Theoretical (inviscid) pressure distributions.

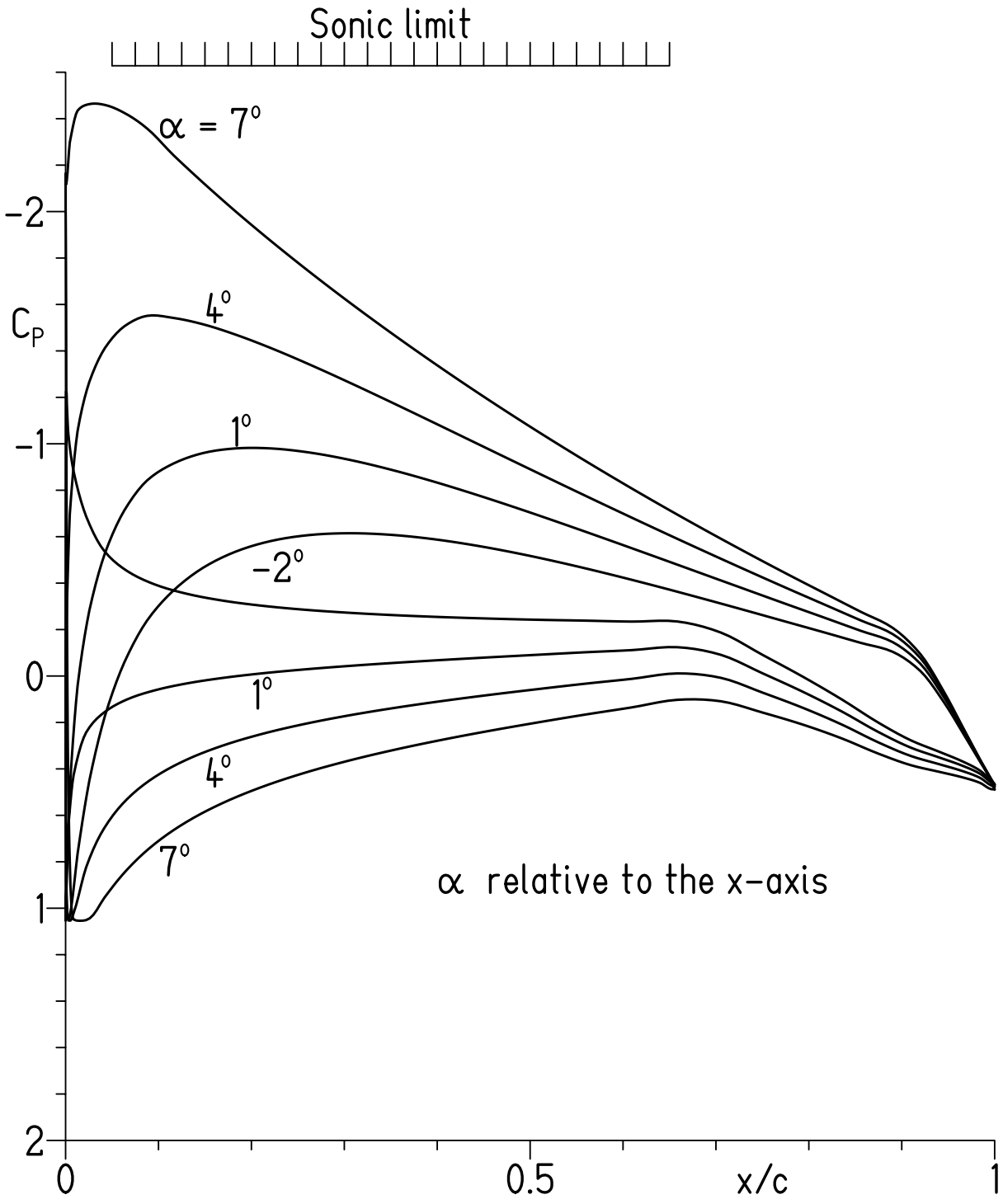

(b) M = 0.46.

Figure 4.- Continued.

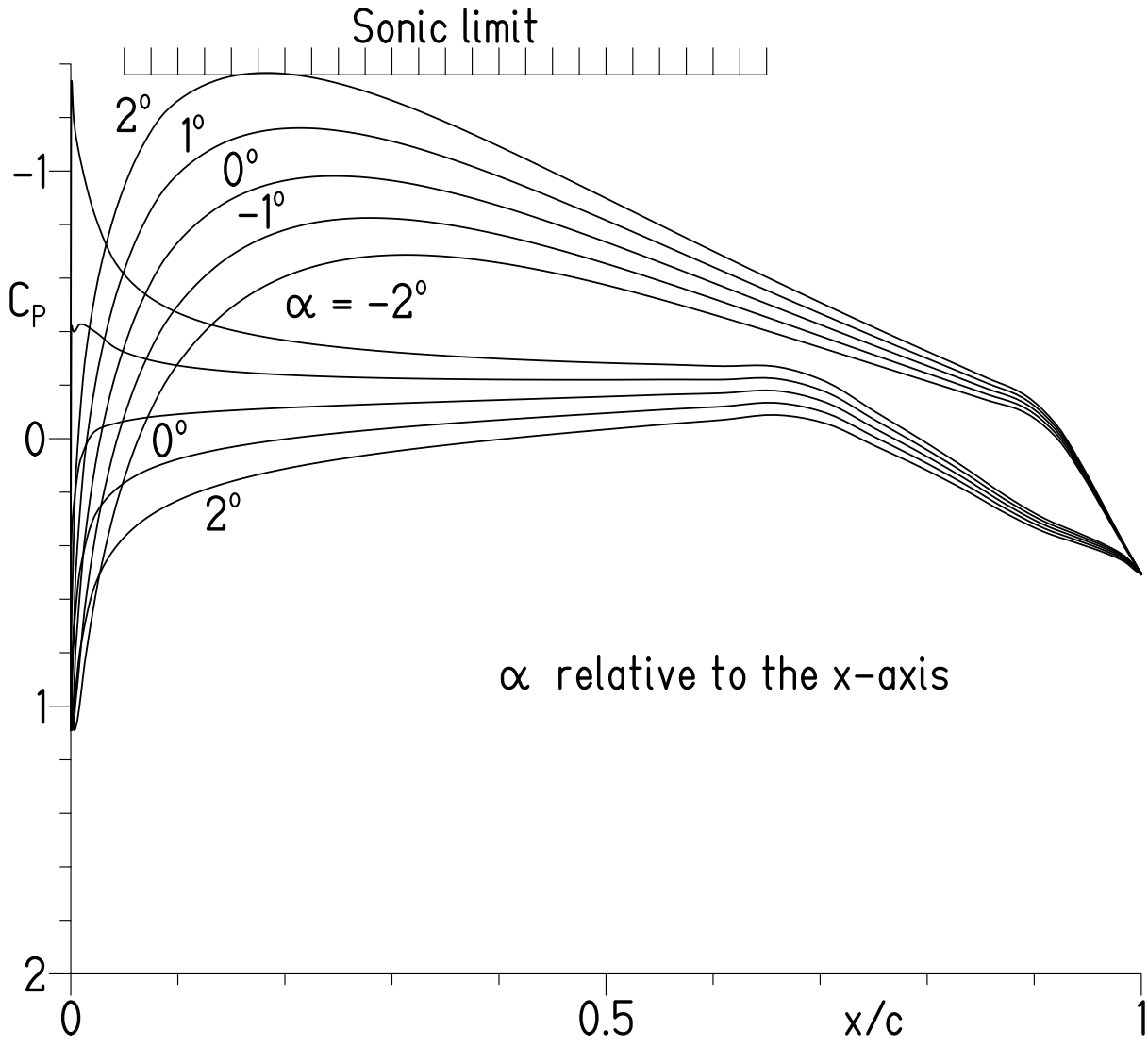

(c) M = 0.59.

Figure 4.- Concluded.

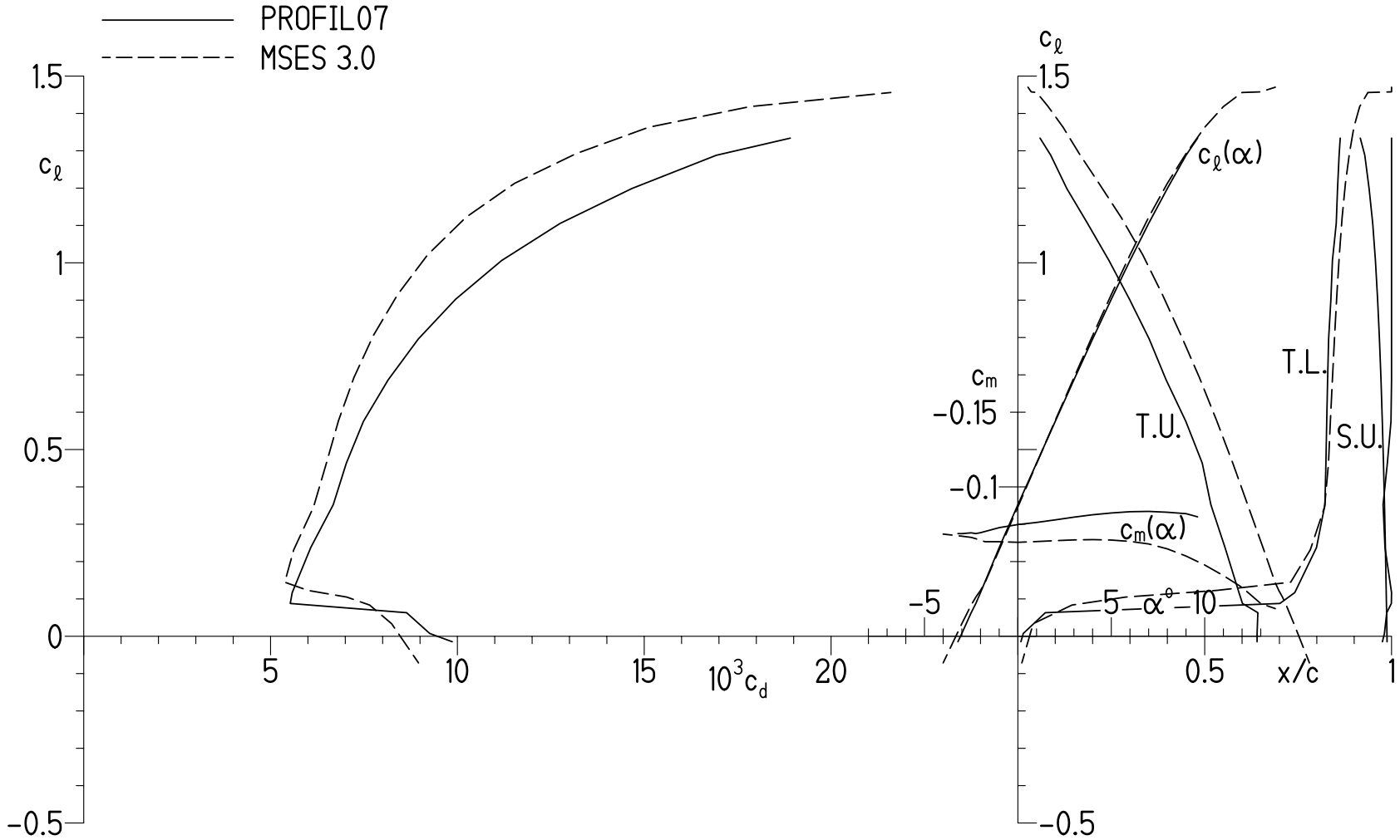

(a) Transition free.

Figure 5.- Theoretical section characteristics at $M = 0.30$ and $R = 1.14 \times 10^6$.

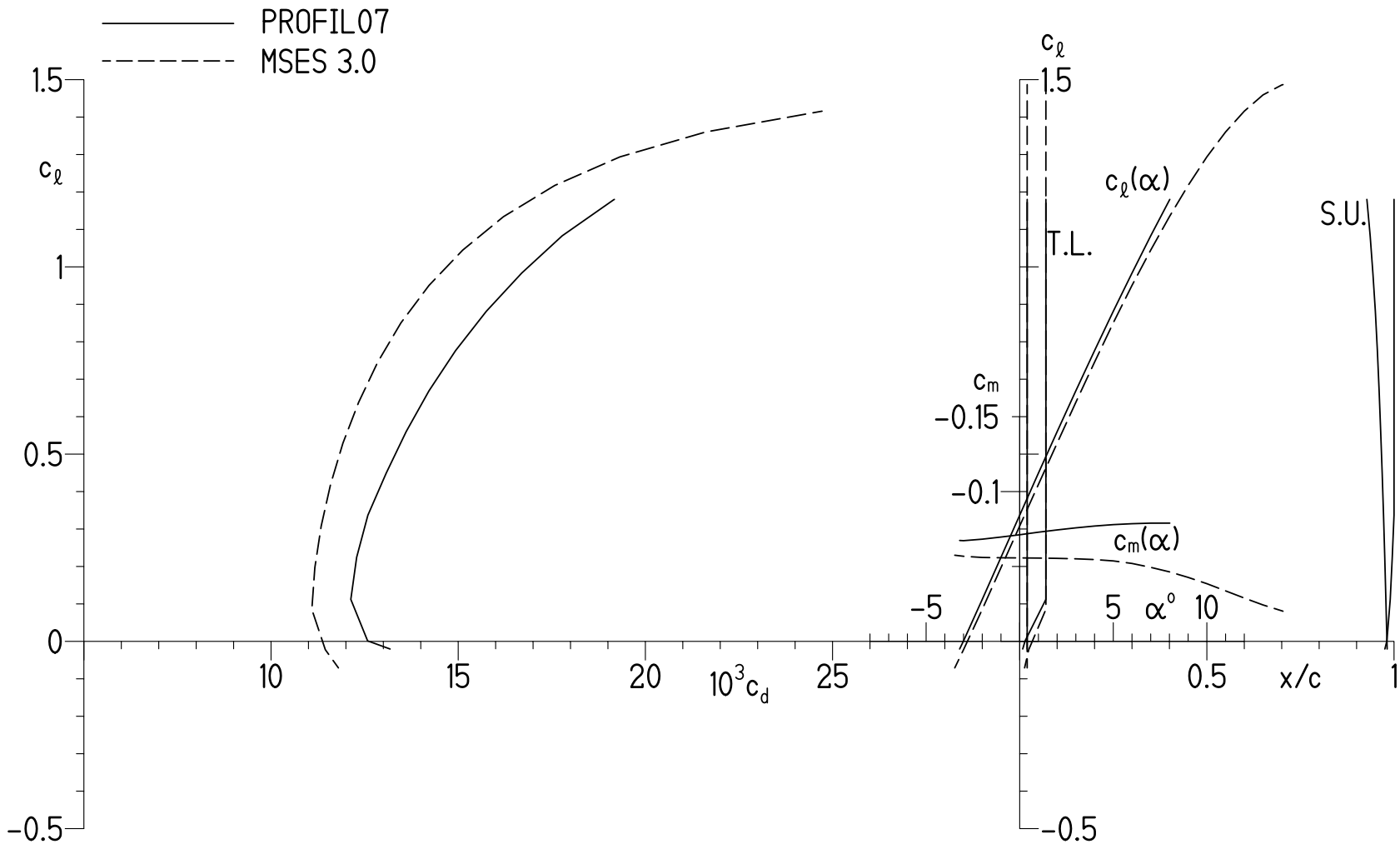

(b) Transition fixed.

Figure 5.- Concluded.

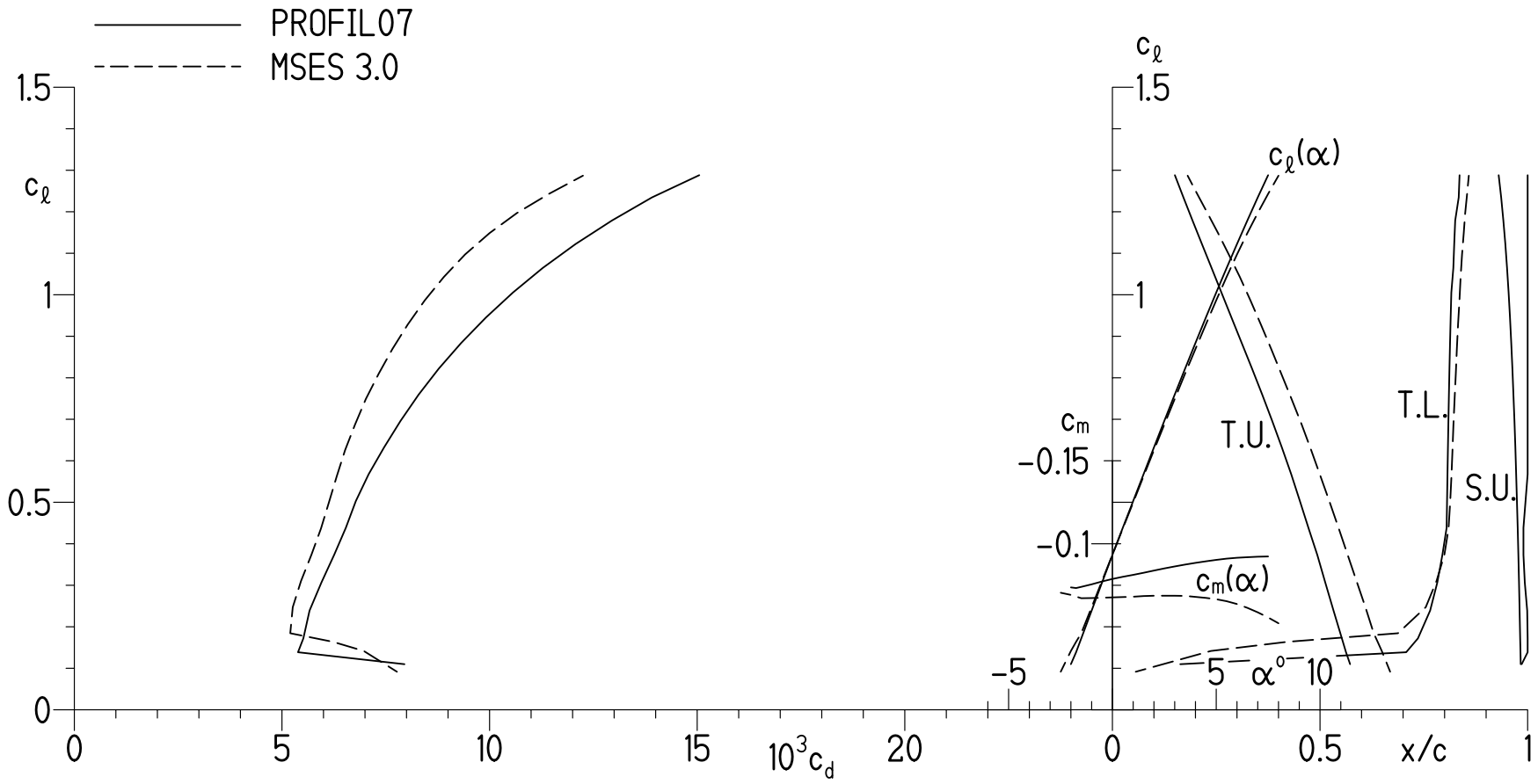

(a) Transition free.

Figure 6.- Theoretical section characteristics at $M = 0.46$ and $R = 1.63 \times 10^6$.

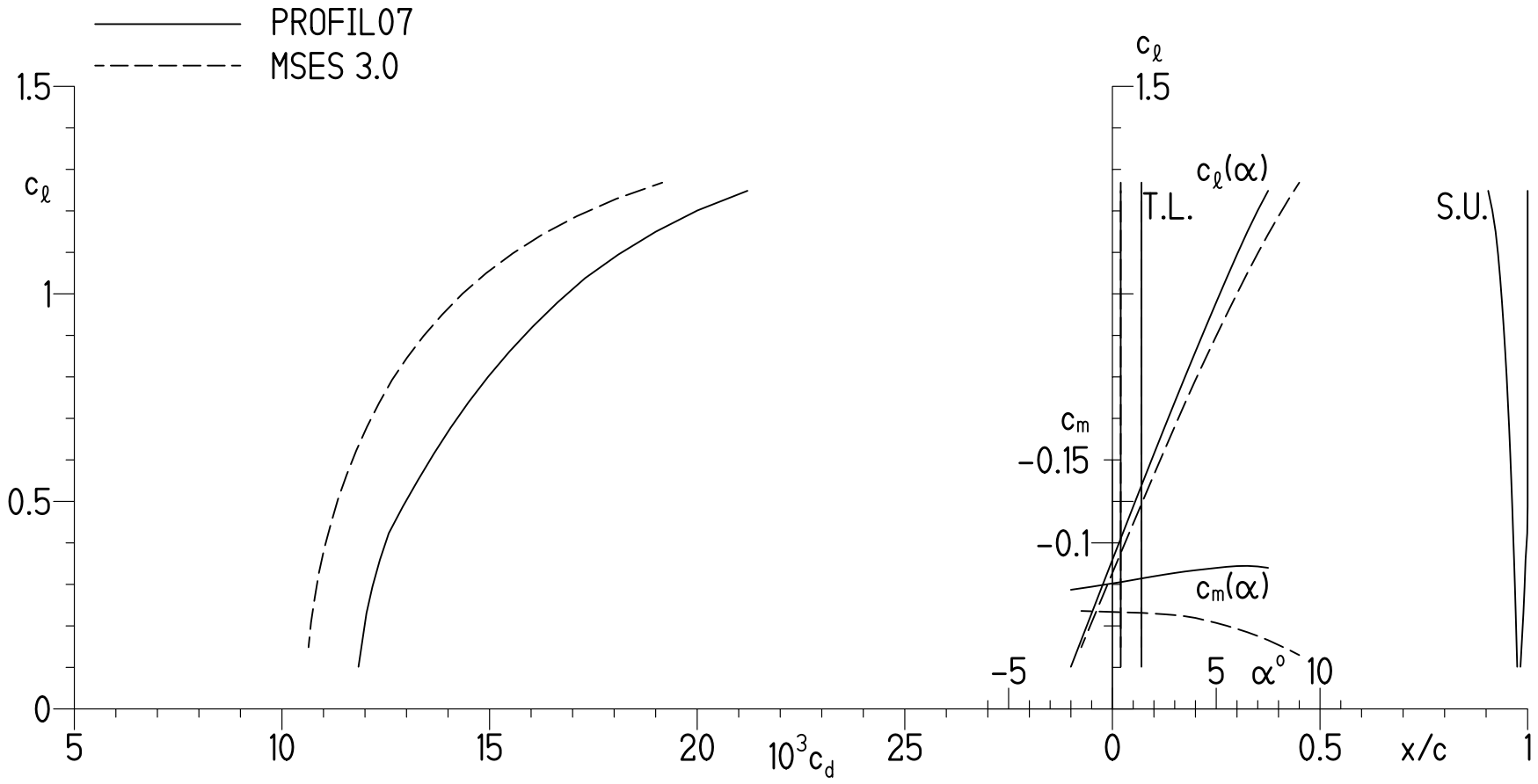

(b) Transition fixed.

Figure 6.- Concluded.

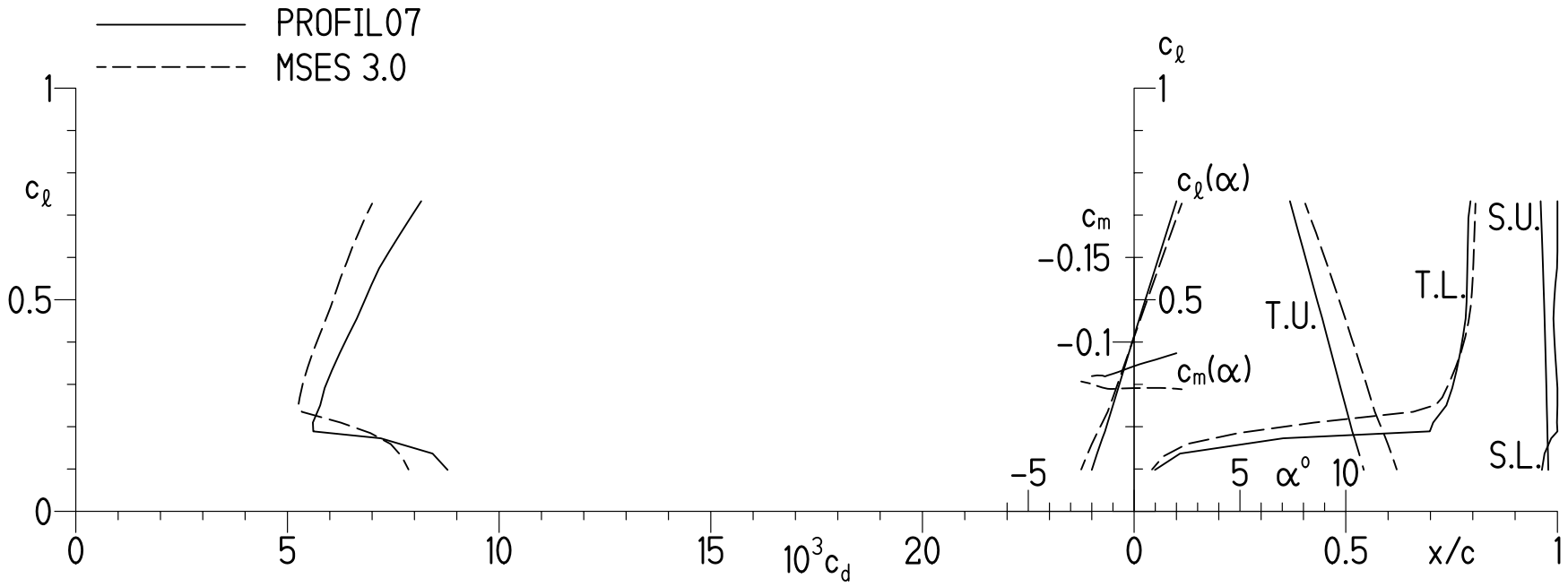

(a) Transition free.

Figure 7.- Theoretical section characteristics at $M = 0.59$ and $R = 2.12 \times 10^6$.

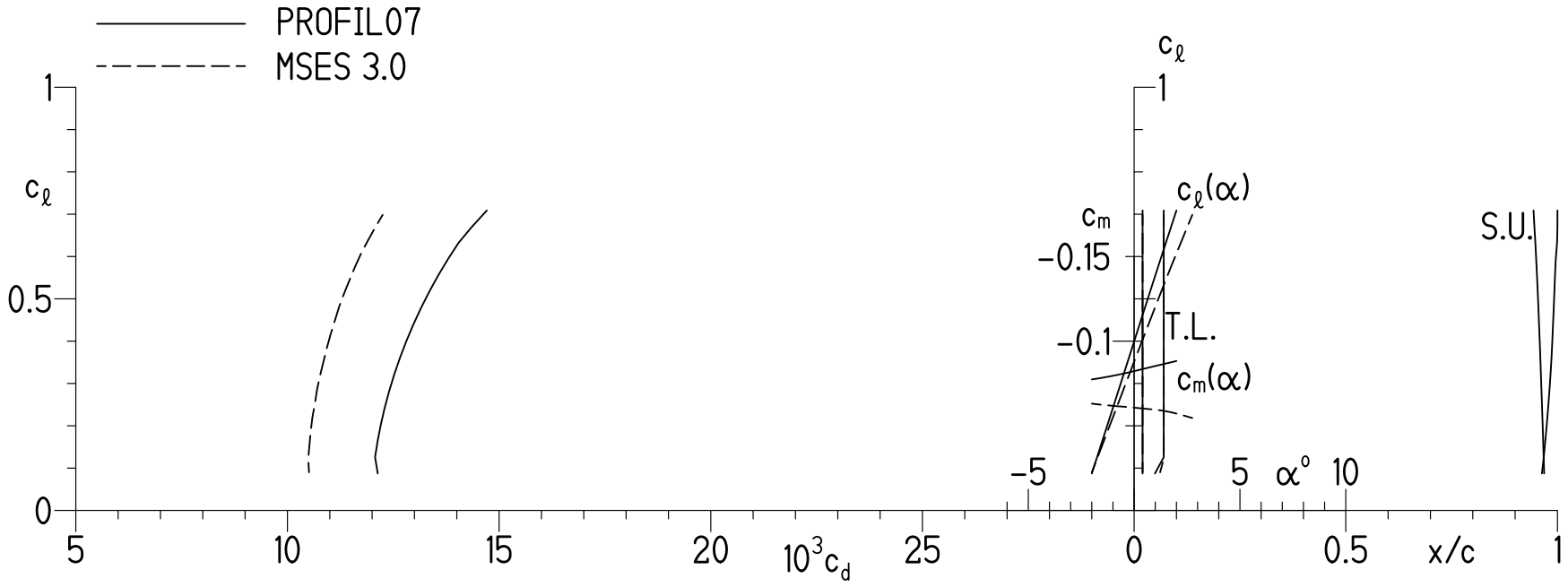

(b) Transition fixed.

Figure 7.- Concluded.

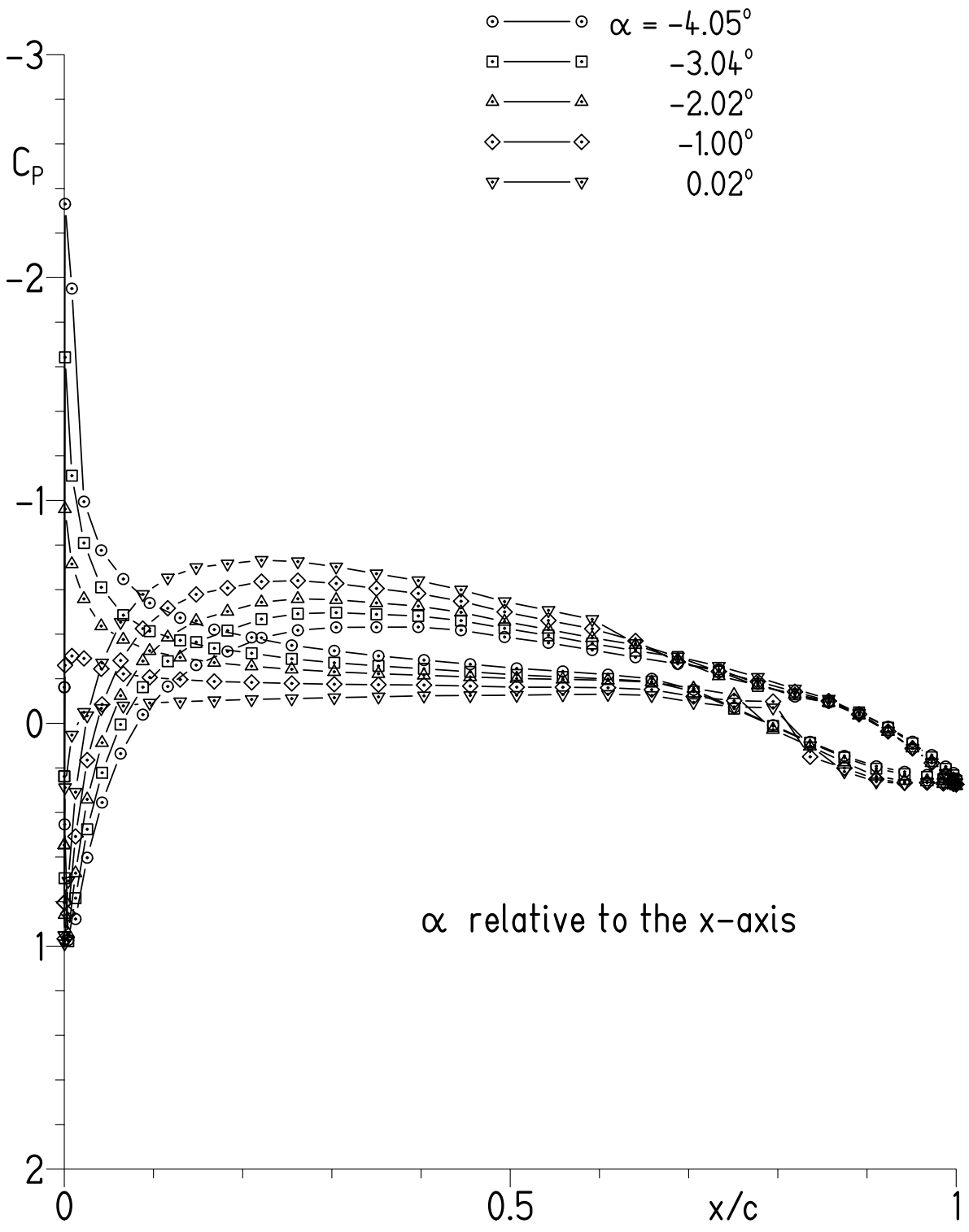

(a) $\alpha = -4.05°, -3.04°, -2.02°, -1.00°$, and $0.02°$.

Figure 8.- Experimental pressure distributions for $R = 1.00 \times 10^6$ and $M = 0.11$ with transition free.

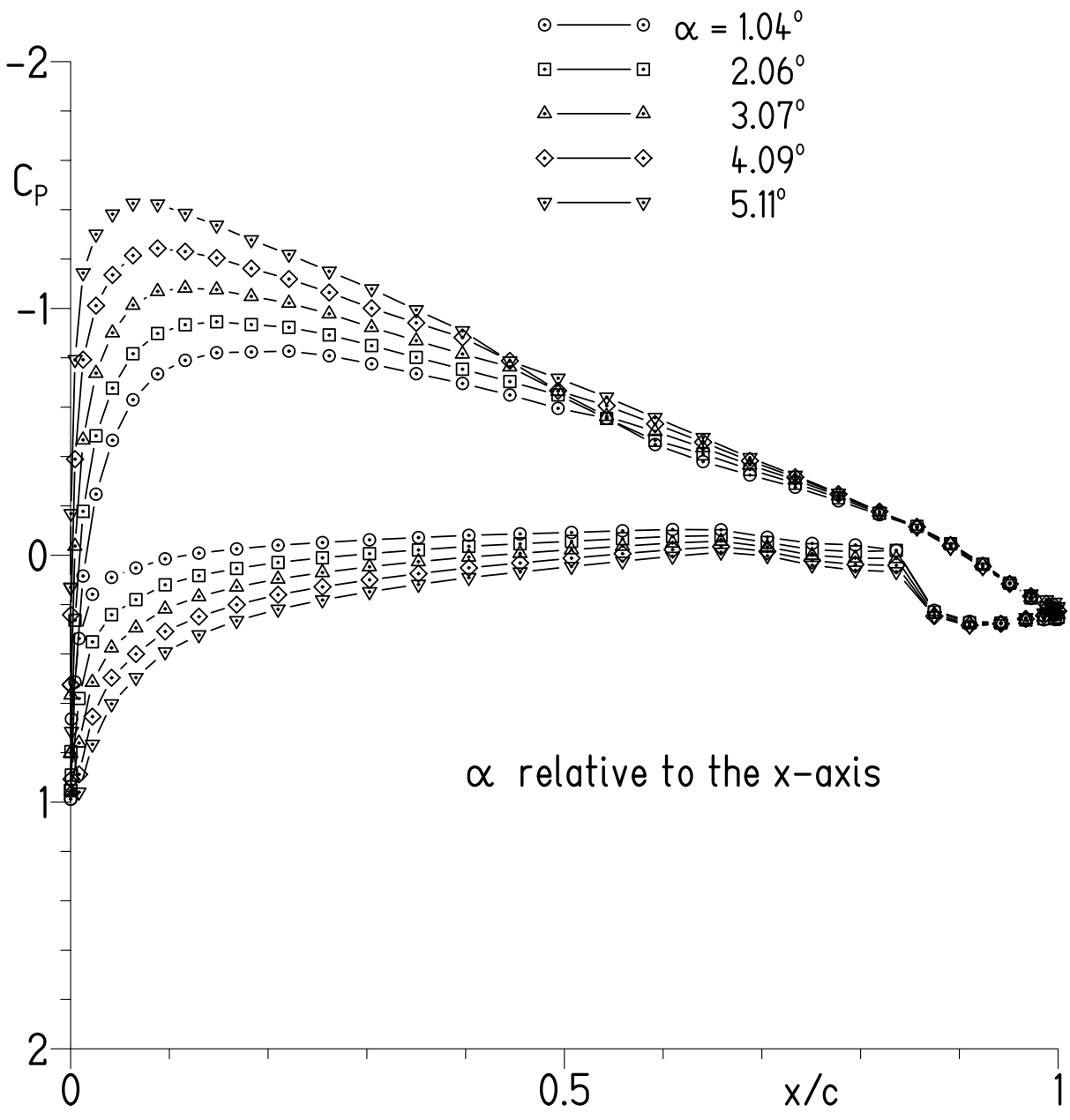

(b) $\alpha = 1.04°, 2.06°, 3.07°, 4.09°$, and $5.11°$.

Figure 8.- Continued.

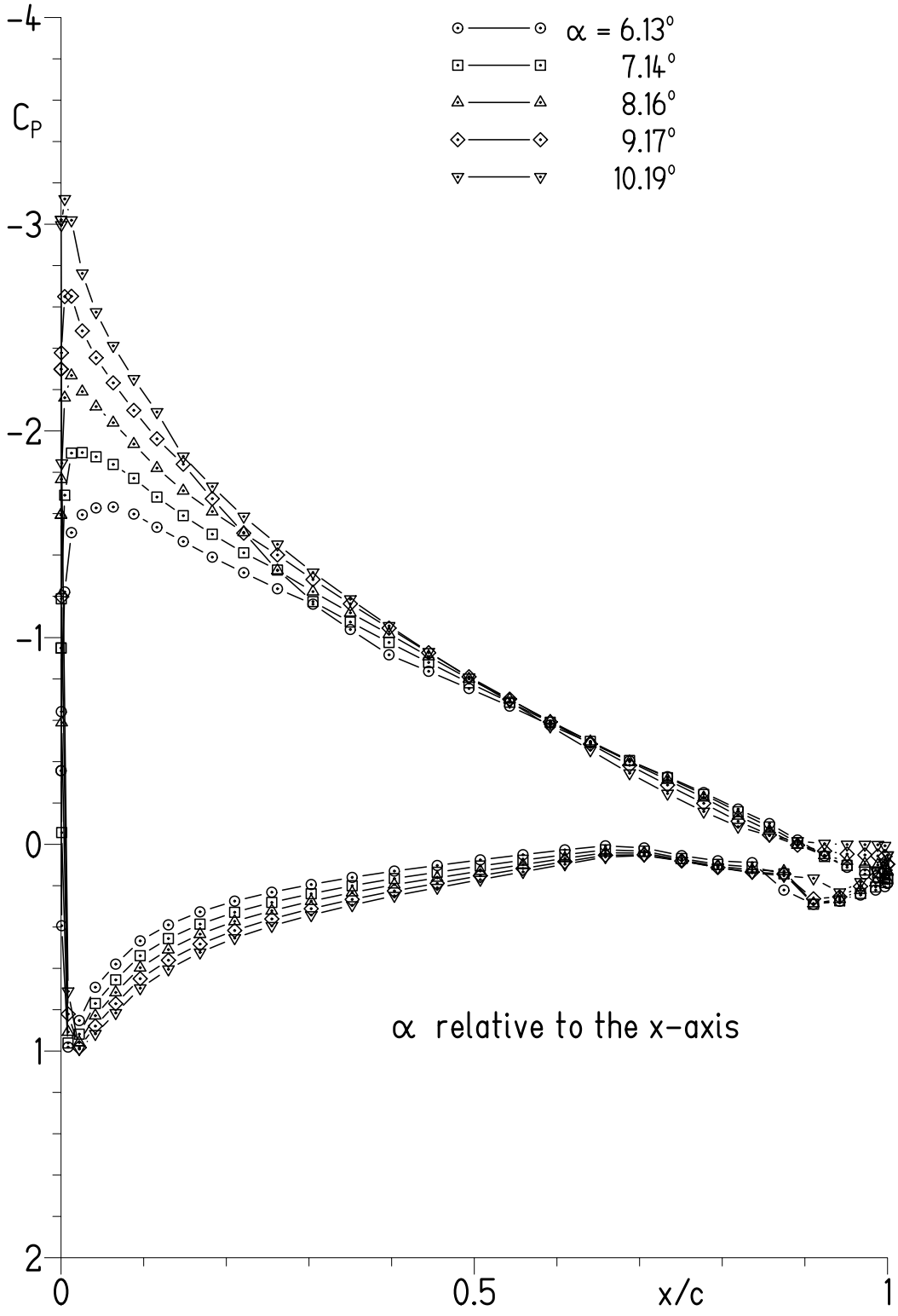

(c) $\alpha = 6.13°$, 7.14°, 8.16°, 9.17°, and 10.19°.

Figure 8.- Continued.

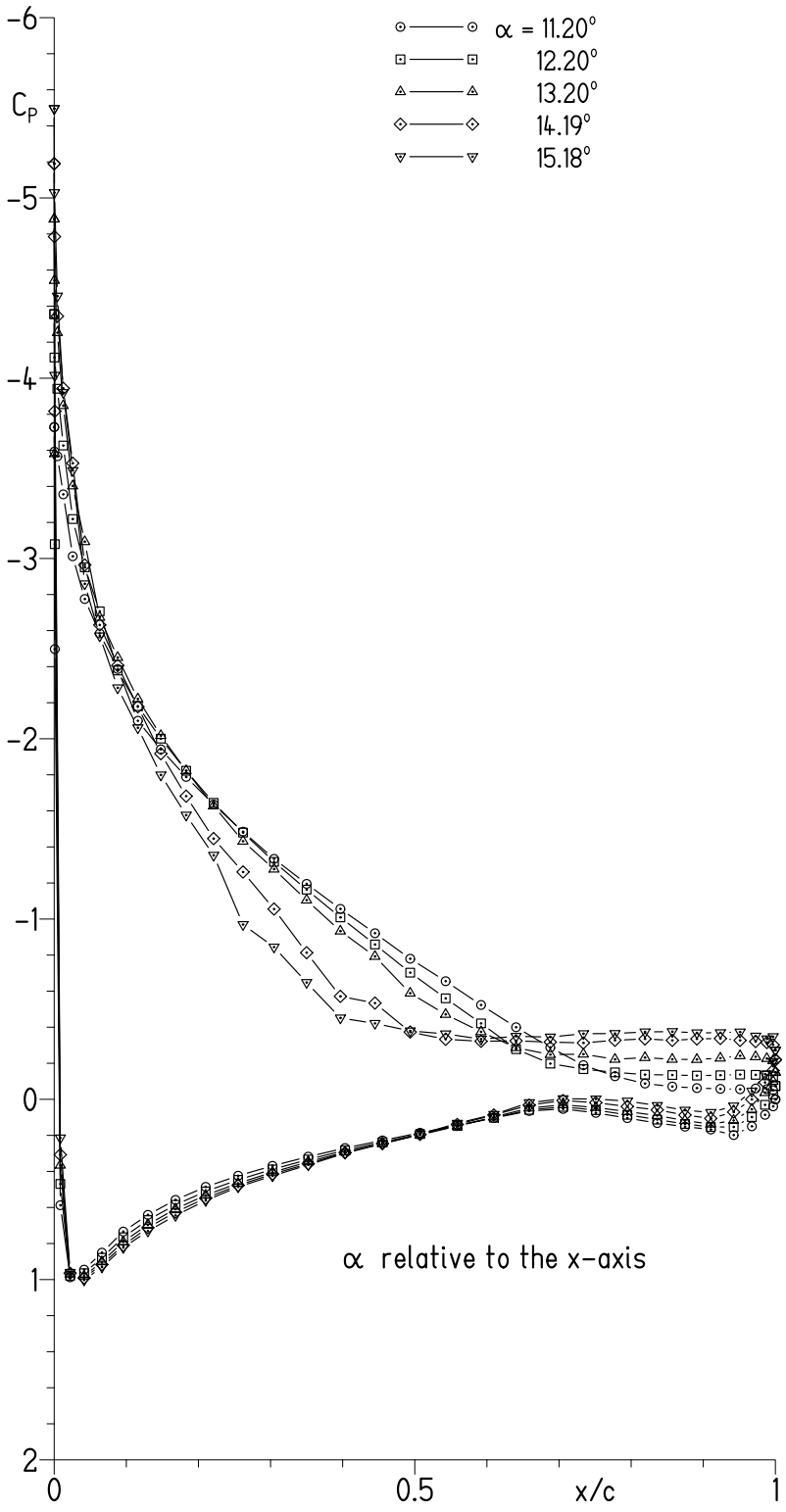

(d) $\alpha = 11.20°, 12.20°, 13.20°, 14.19°$, and $15.18°$.

Figure 8.- Continued.

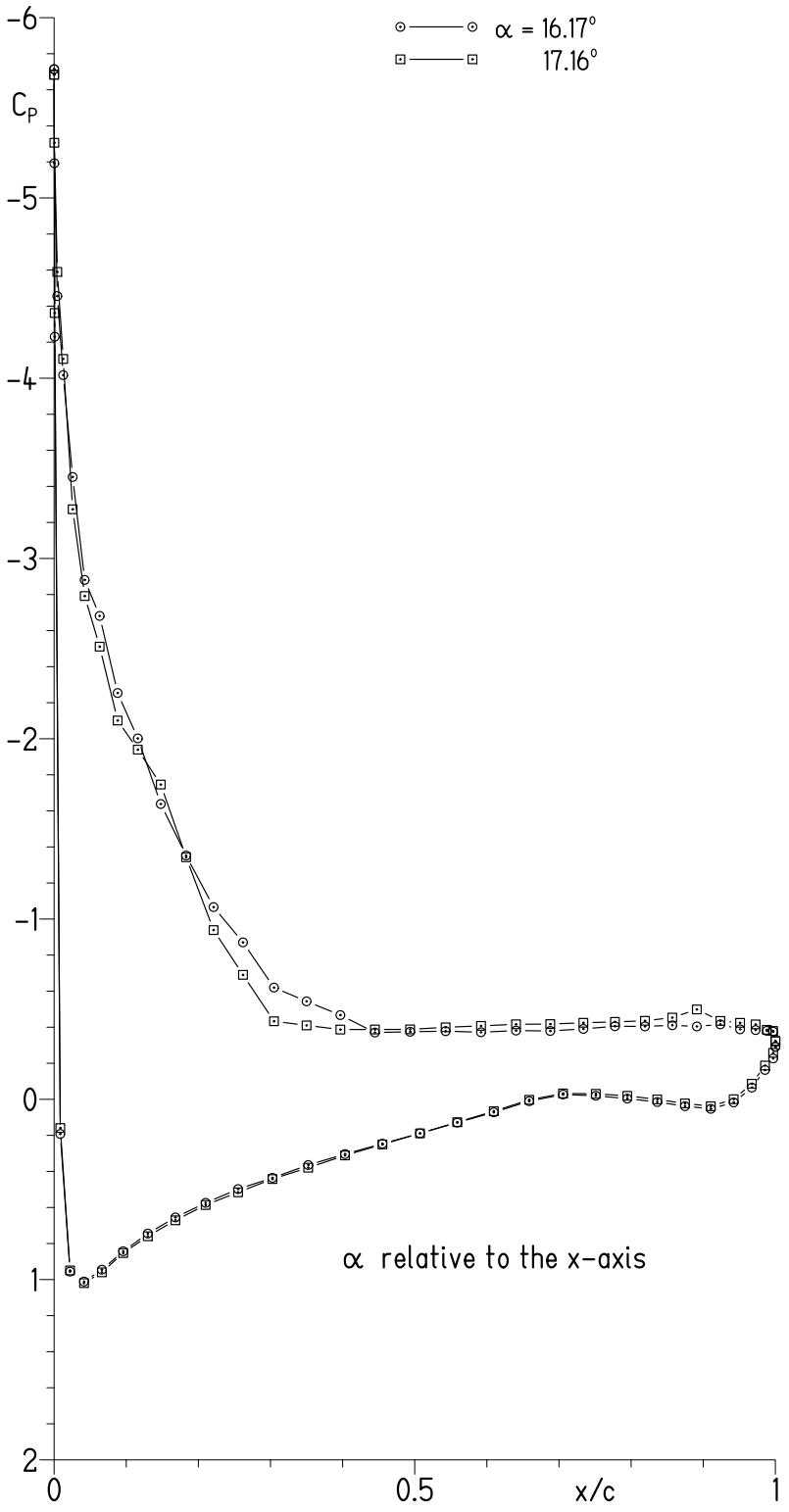

(e) $\alpha = 16.17°$ and $17.16°$.

Figure 8.- Concluded.

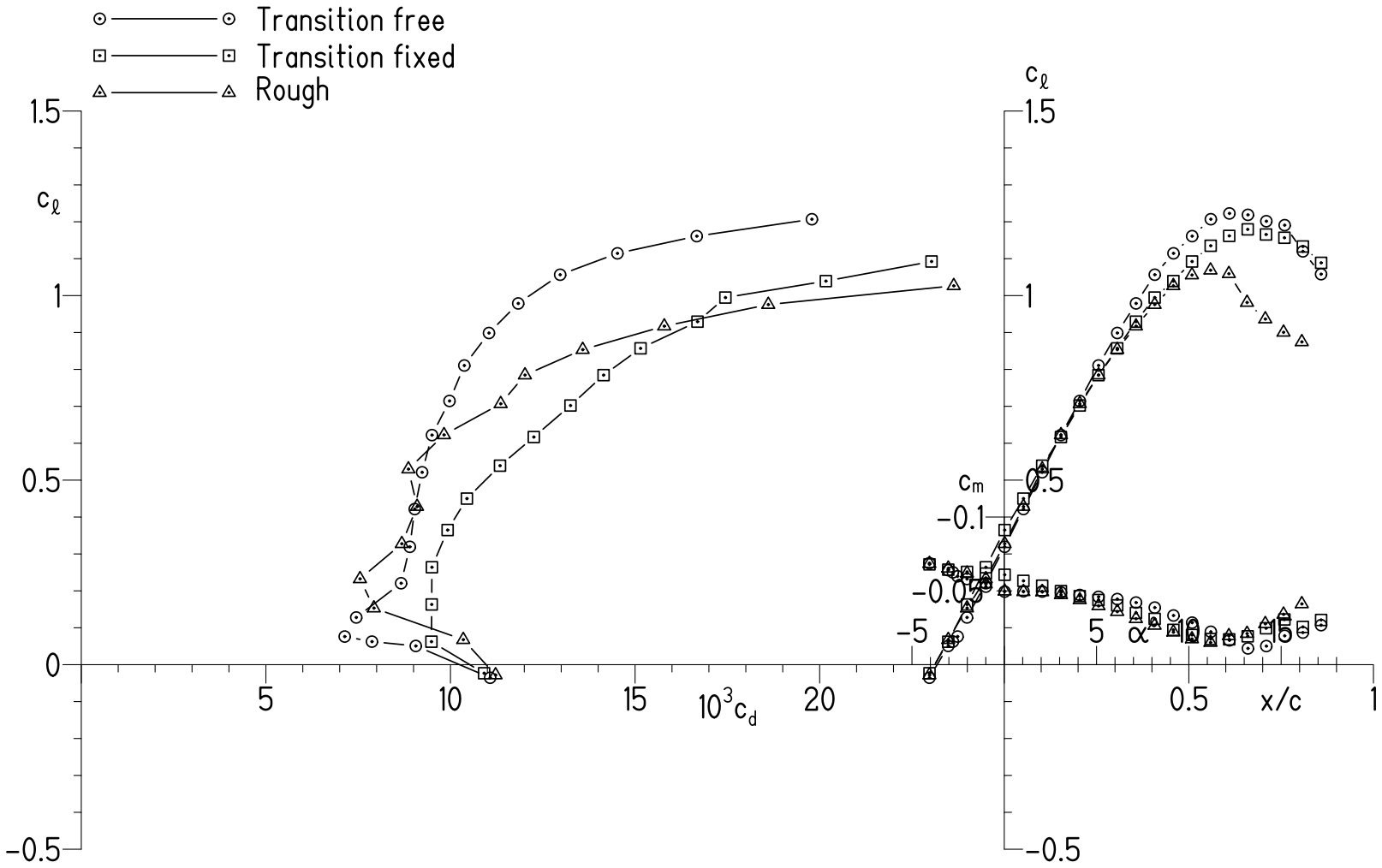

(a) $R = 0.50 \times 10^6$ and $M = 0.05$.

Figure 9.- Experimental section characteristics with transition free, transition fixed, and rough.

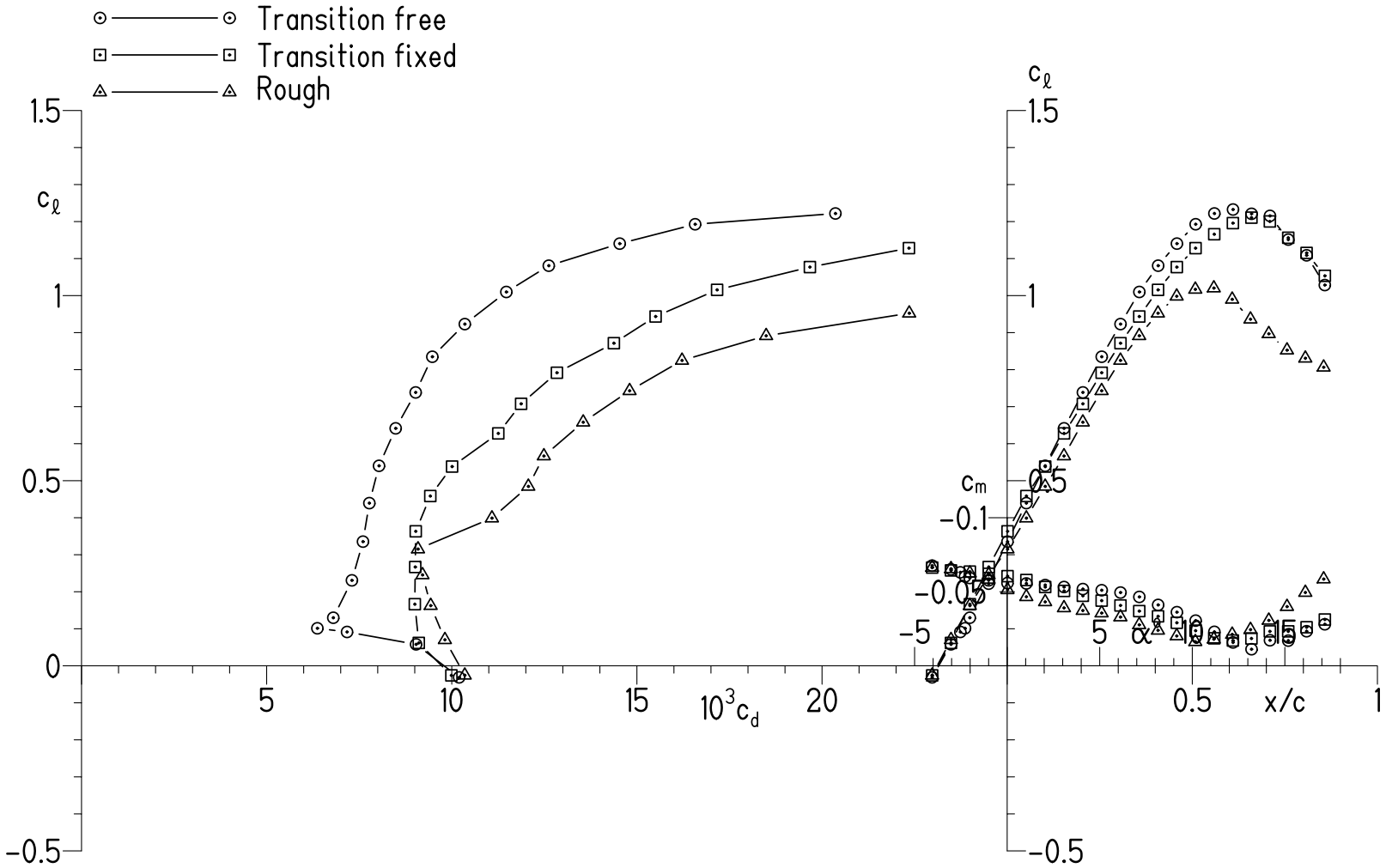

(b) $R = 0.70 \times 10^6$ and $M = 0.07$.

Figure 9.- Continued.

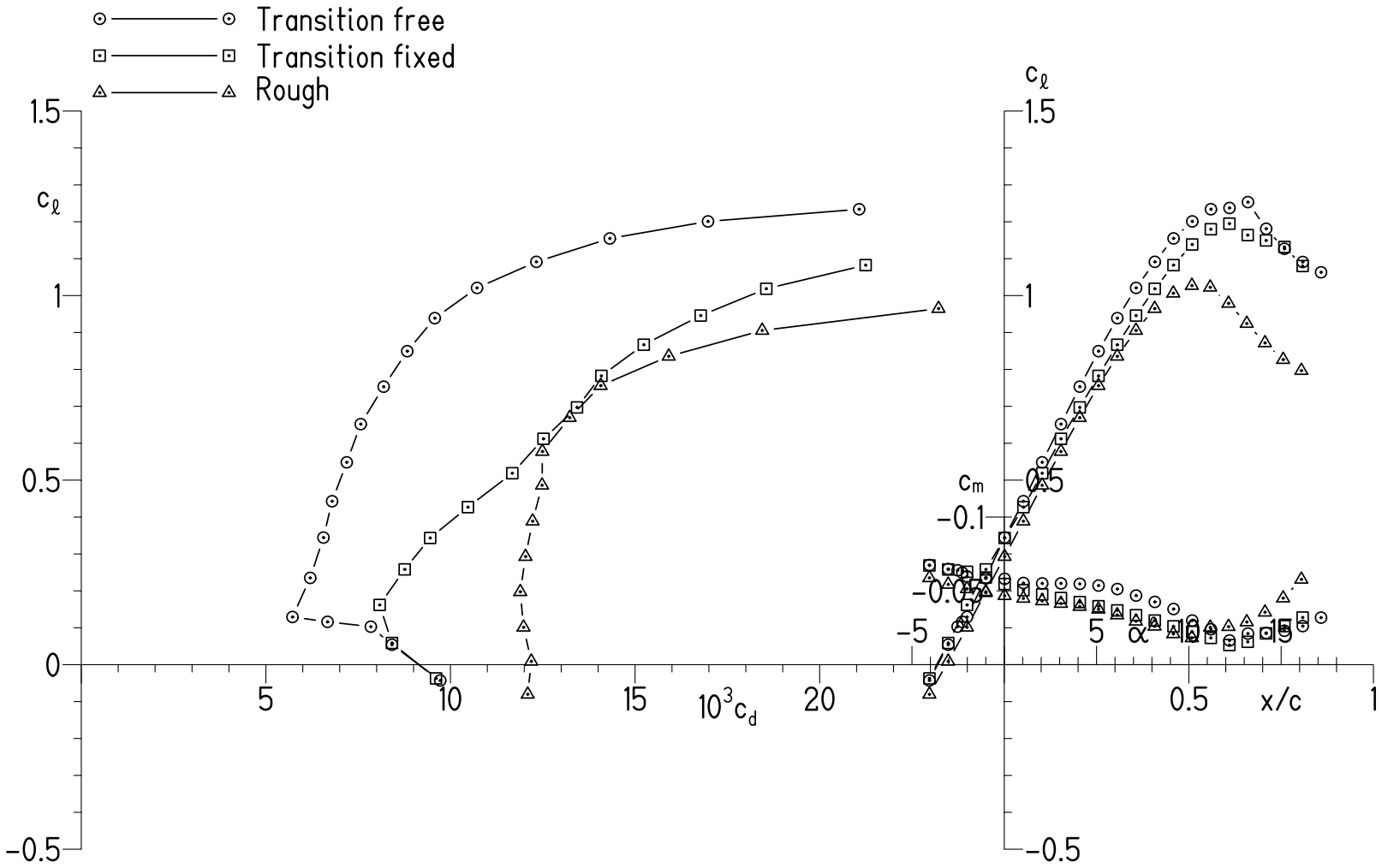

(c) $R = 1.00 \times 10^6$ and $M = 0.11$.

Figure 9.- Continued.

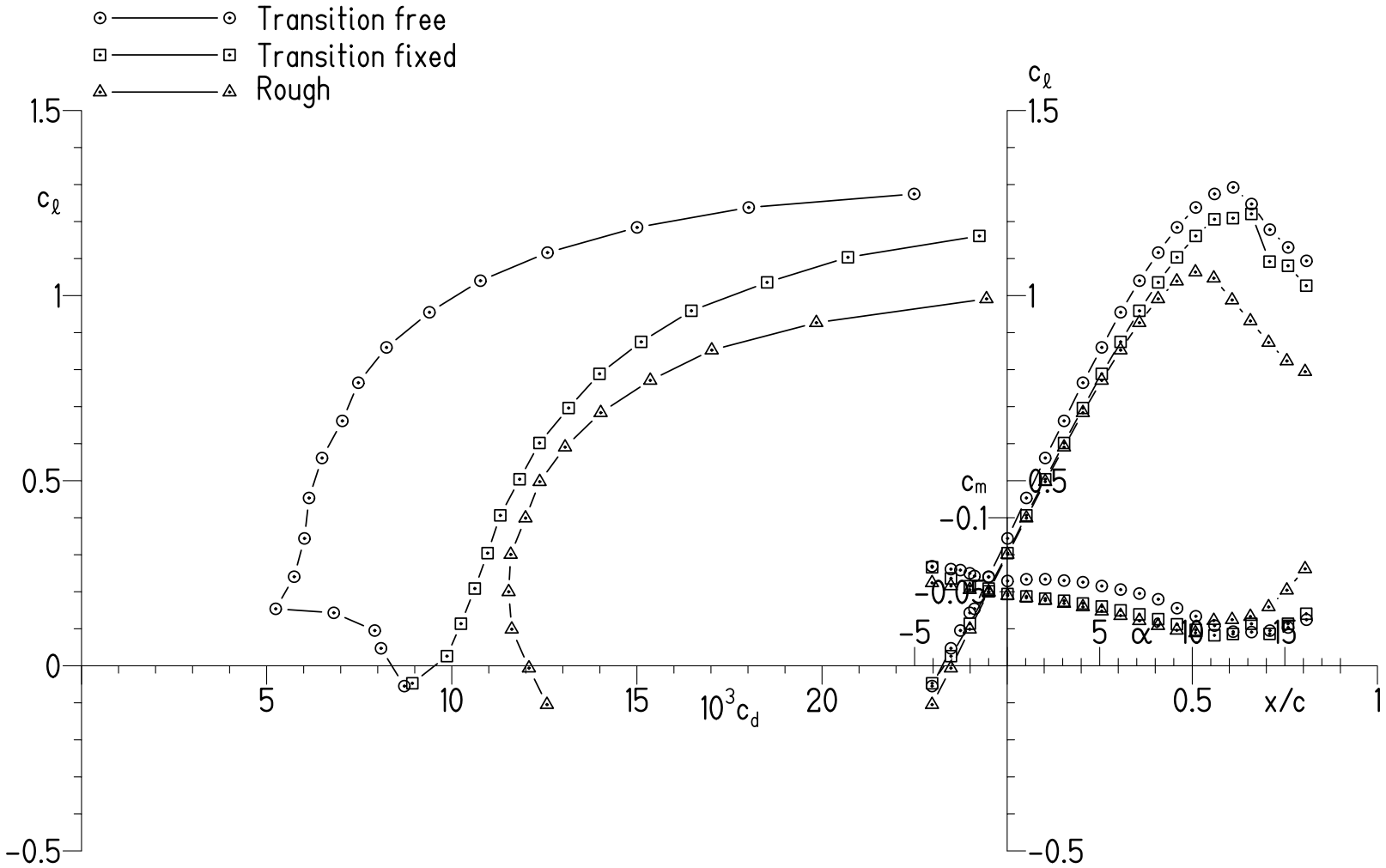

(d) $R = 1.50 \times 10^6$ and $M = 0.17$.

Figure 9.- Concluded.

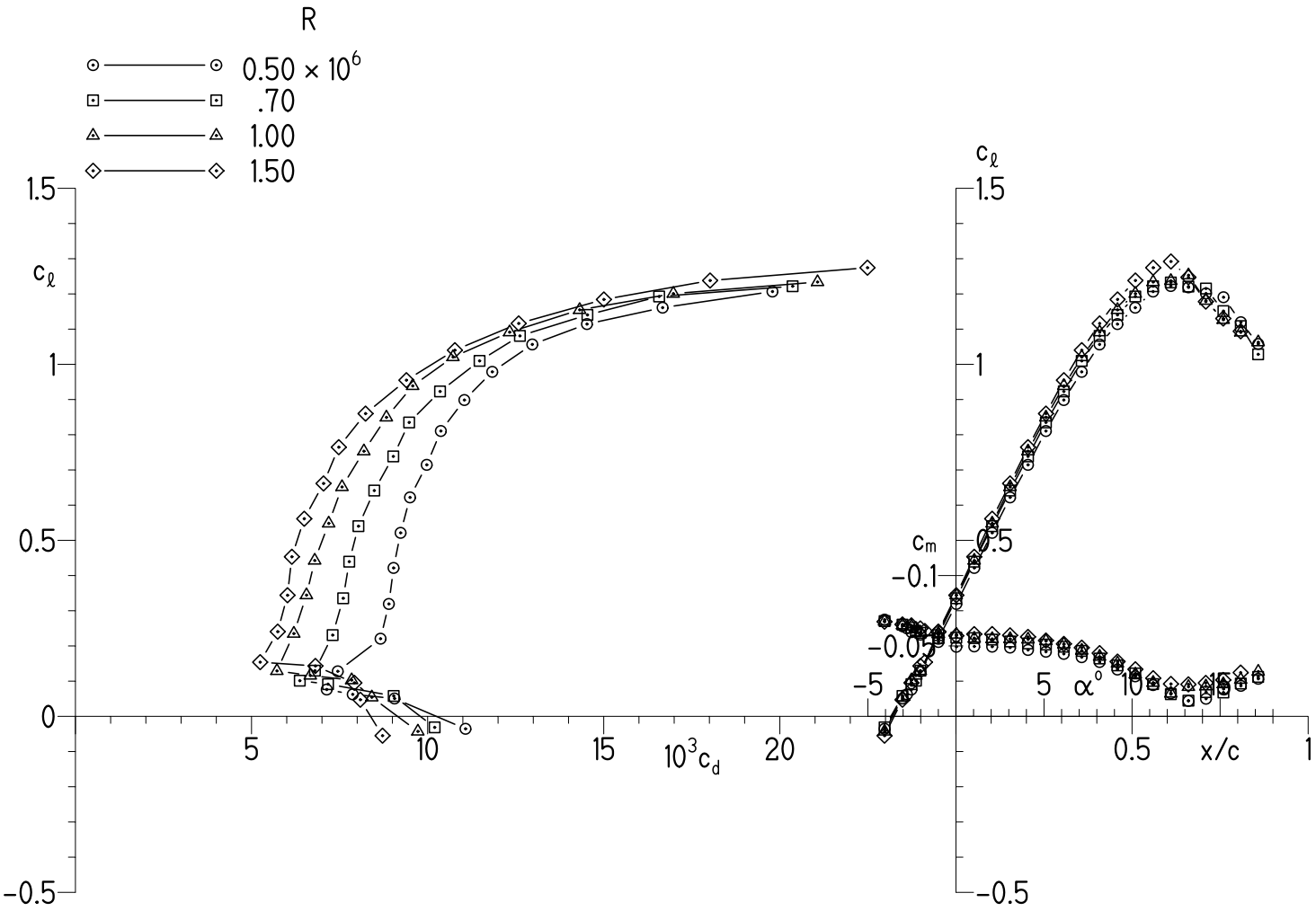

(a) Transition free.

Figure 10.- Effects of Reynolds number on experimental section characteristics.

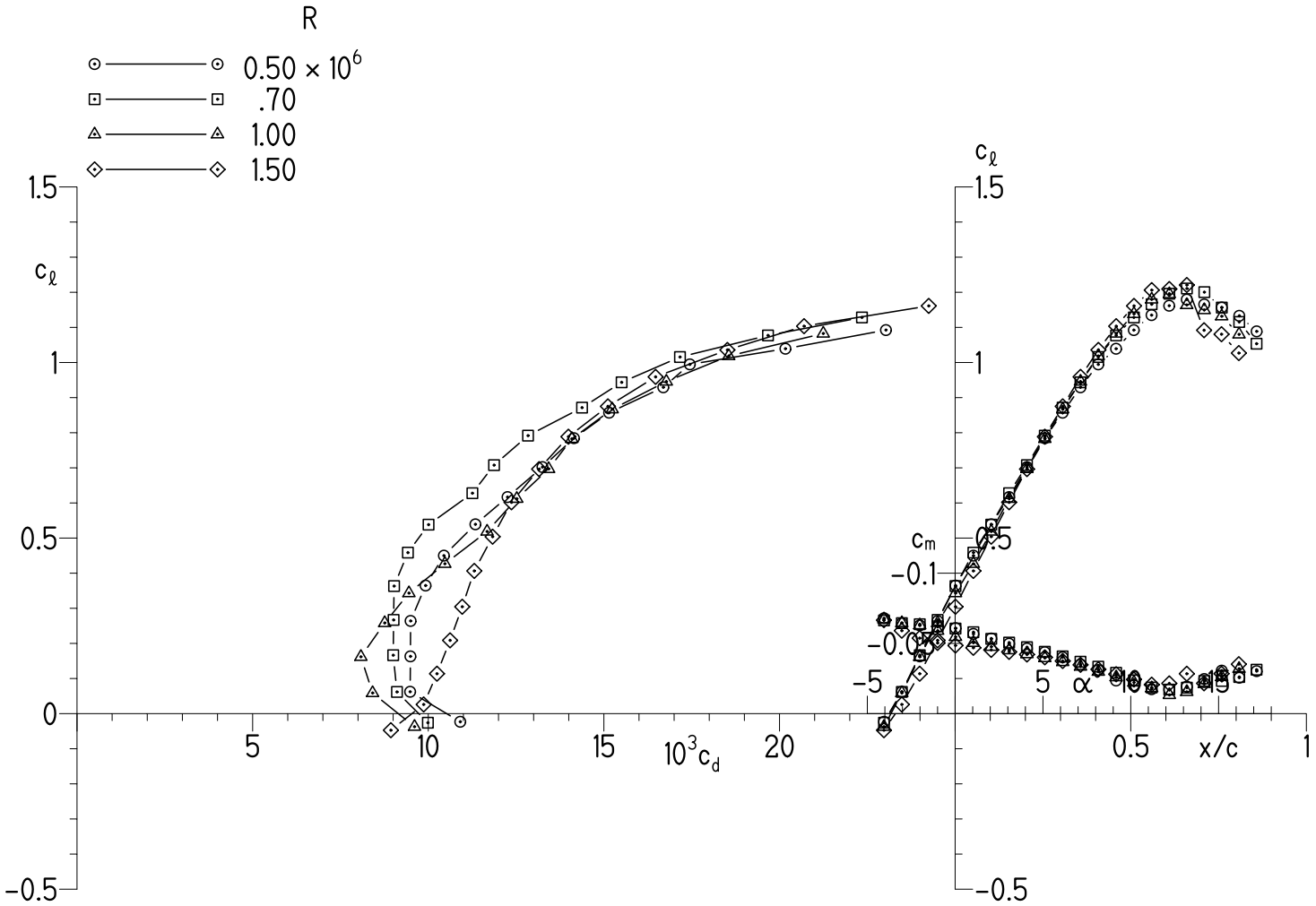

(b) Transition fixed.

Figure 10.- Continued.

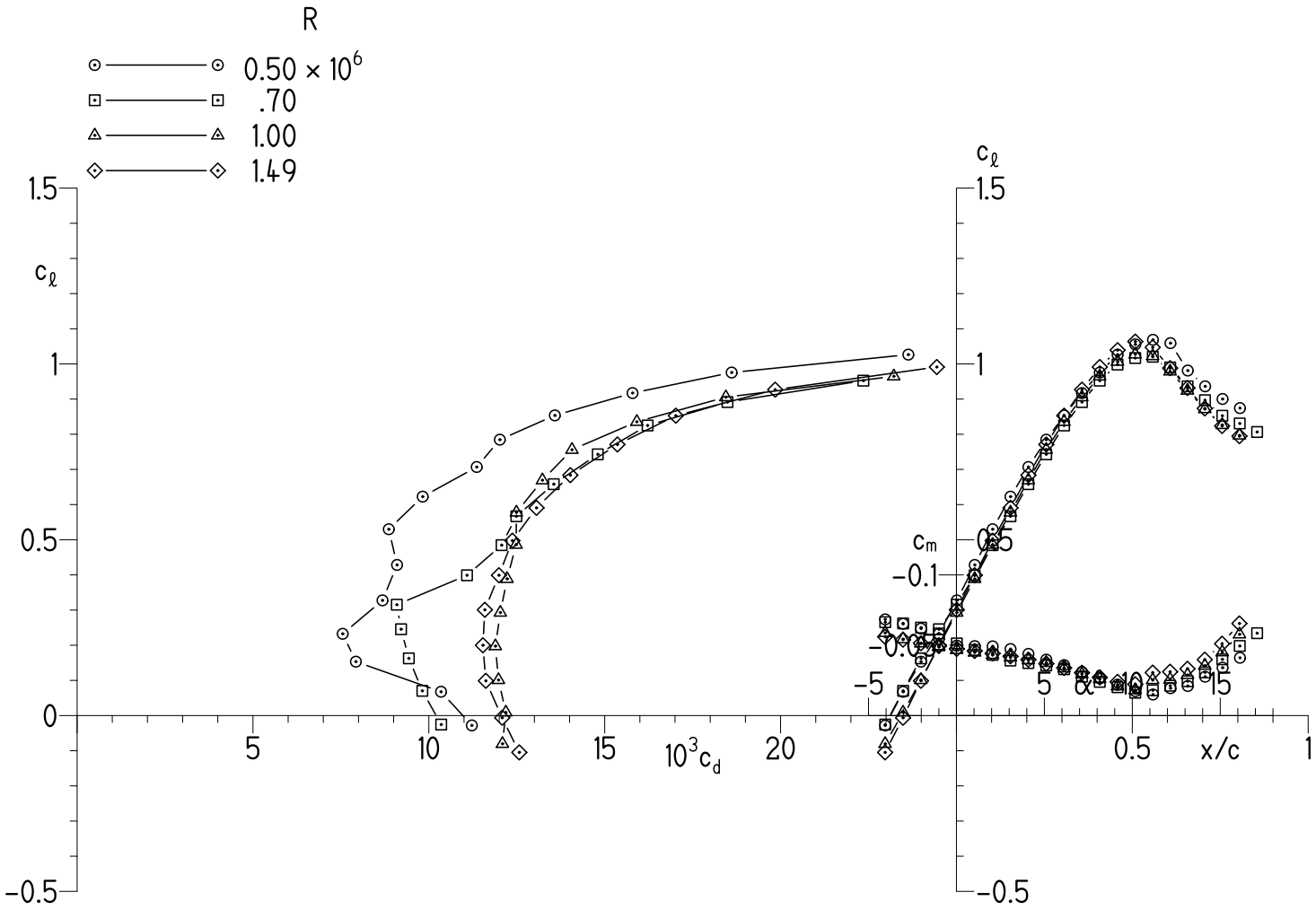

(c) Rough.

Figure 10.- Concluded.

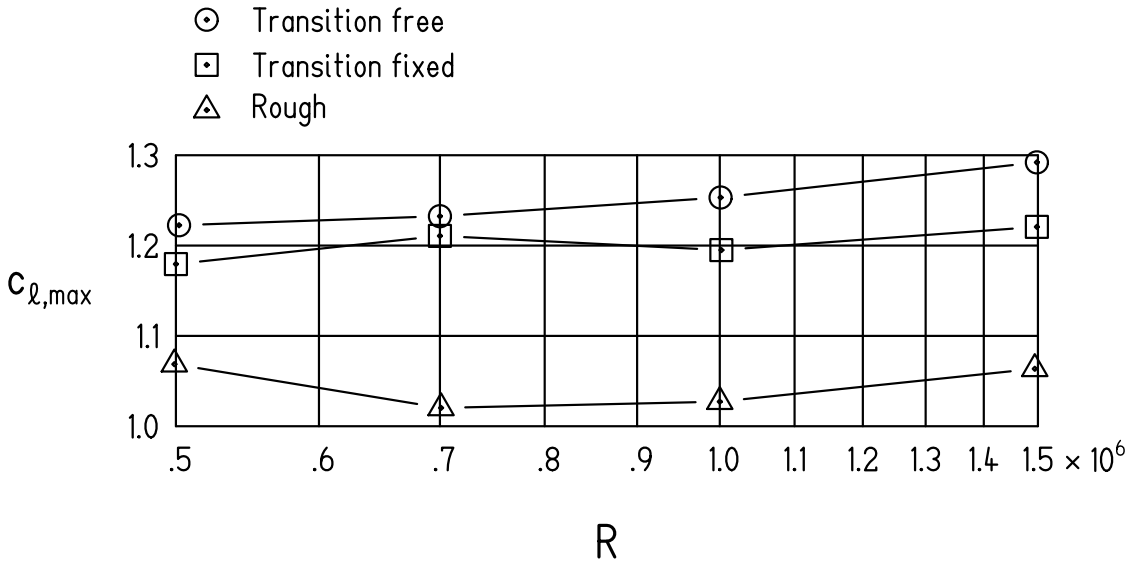

Figure 11.- Variation of experimental maximum lift coefficient with Reynolds number.

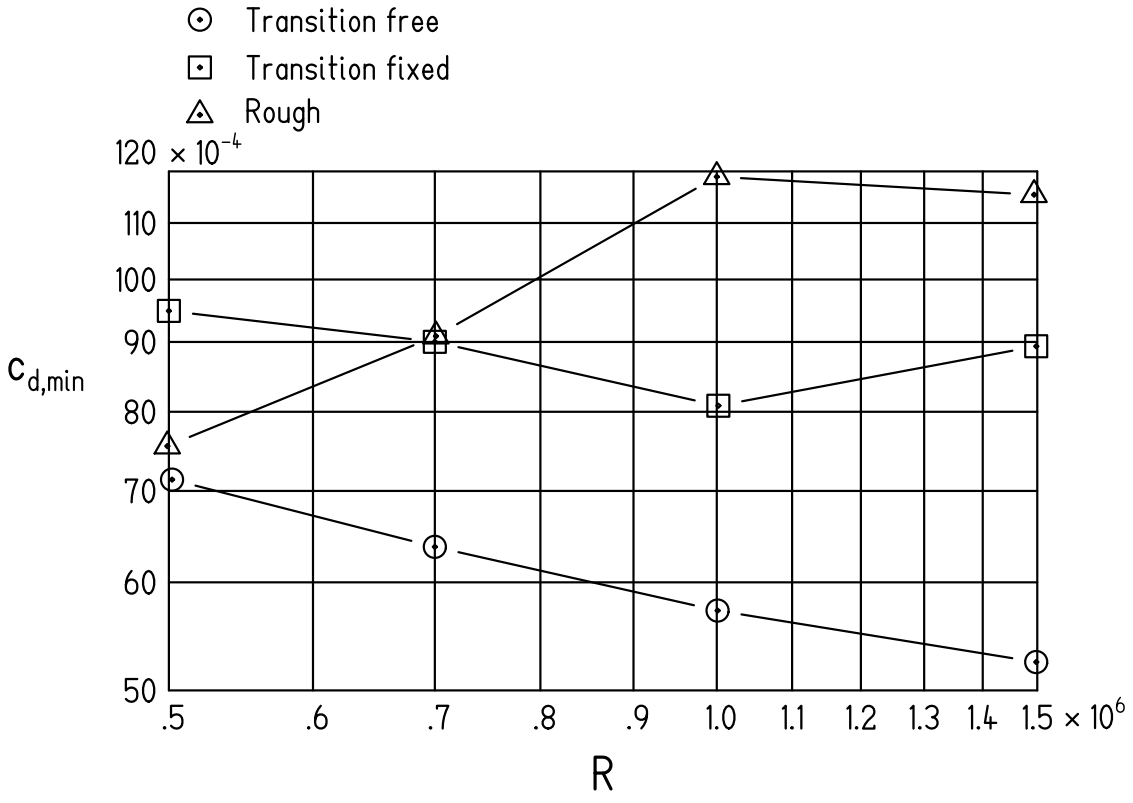

Figure 12.- Variation of experimental minimum profile-drag coefficient with Reynolds number.

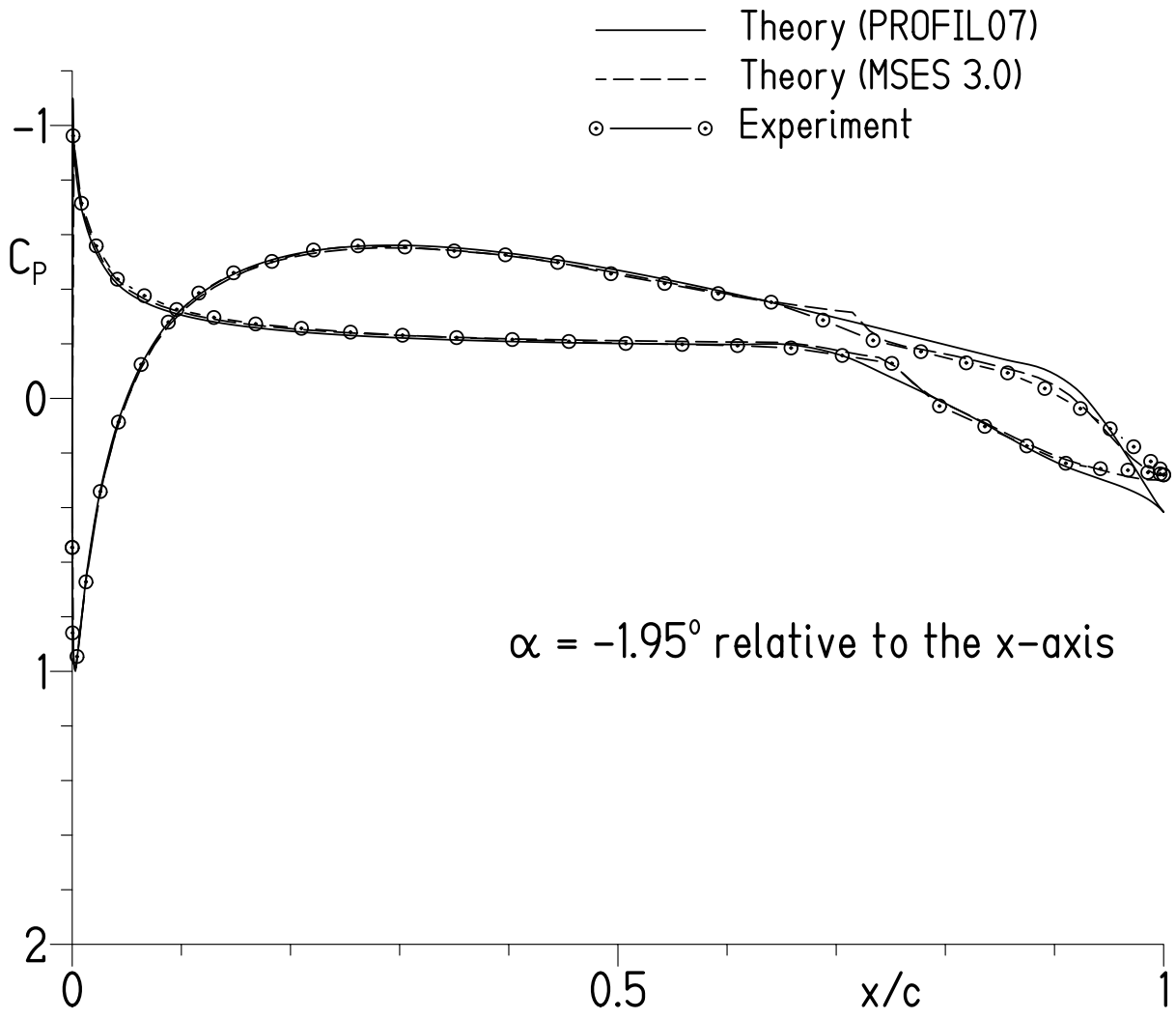

(a) $c_l = 0.13$.

Figure 13.- Comparison of theoretical and experimental pressure distributions.

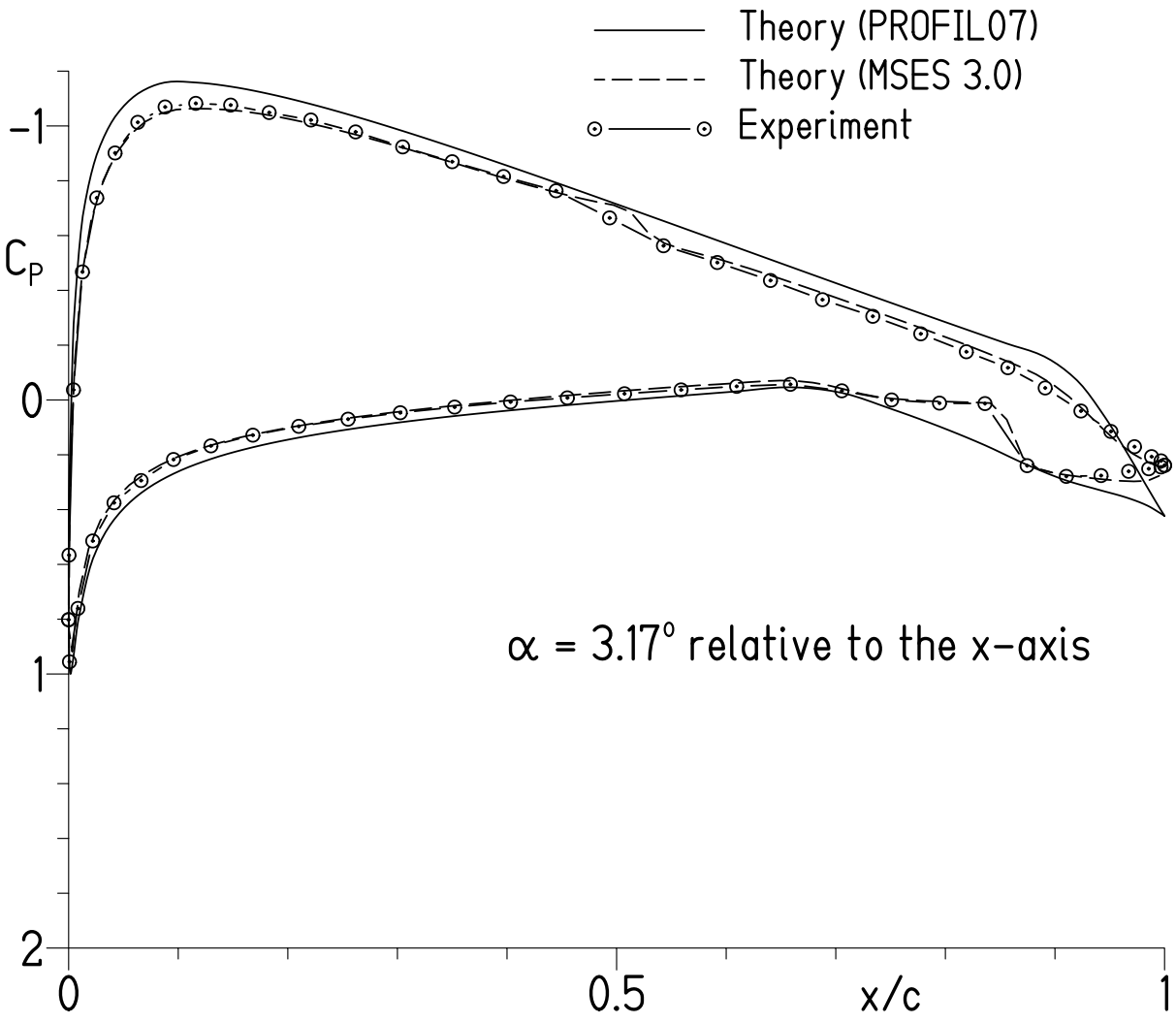

(b) $c_l = 0.67$.

Figure 13.- Continued.

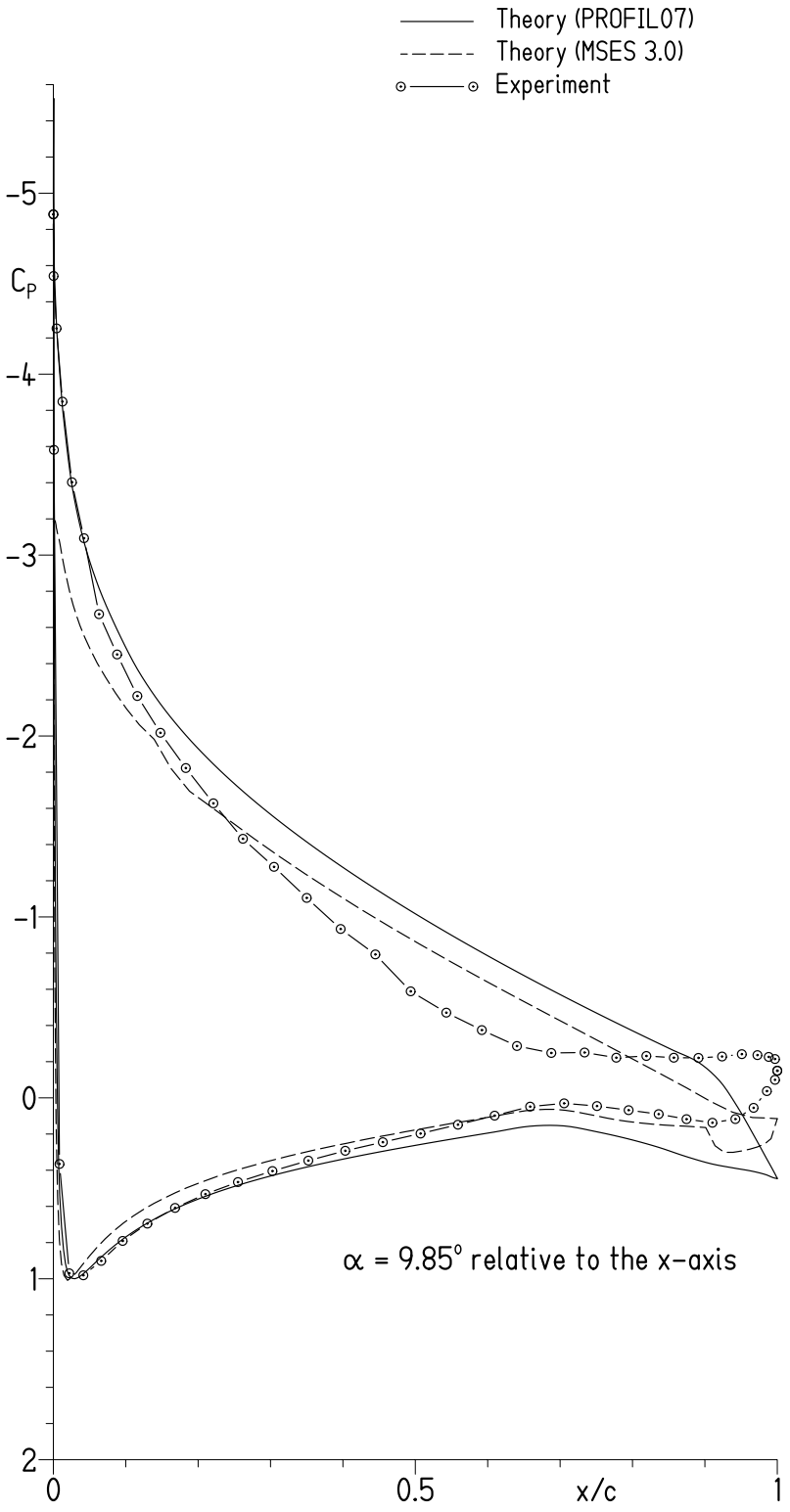

(c) $c_l = c_{l,max}$.

Figure 13.- Concluded.

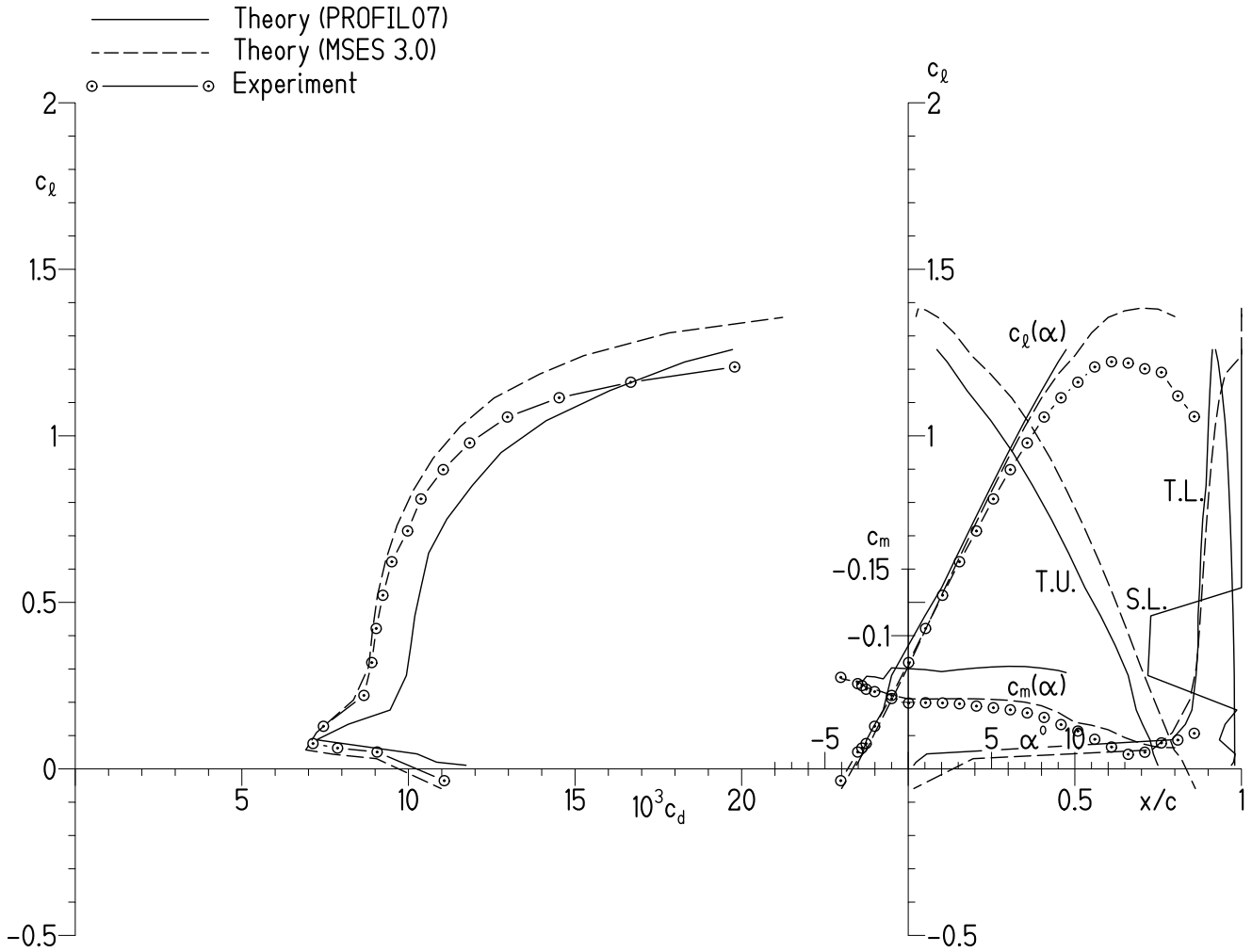

(a) $R = 0.50 \times 10^6$.

Figure 14.- Comparison of theoretical and experimental section characteristics with transition free.

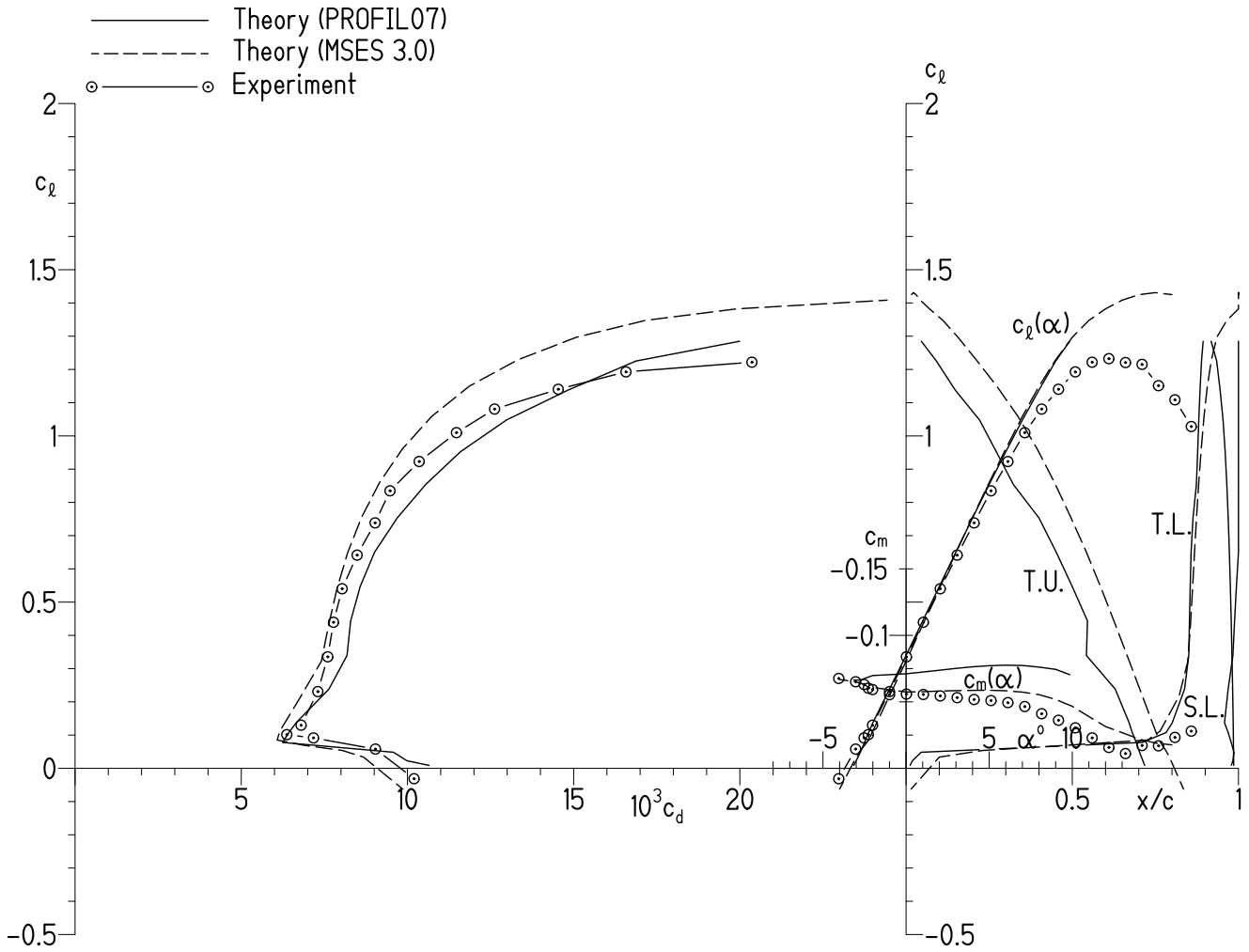

(b) $R = 0.70 \times 10^6$.

Figure 14.- Continued.

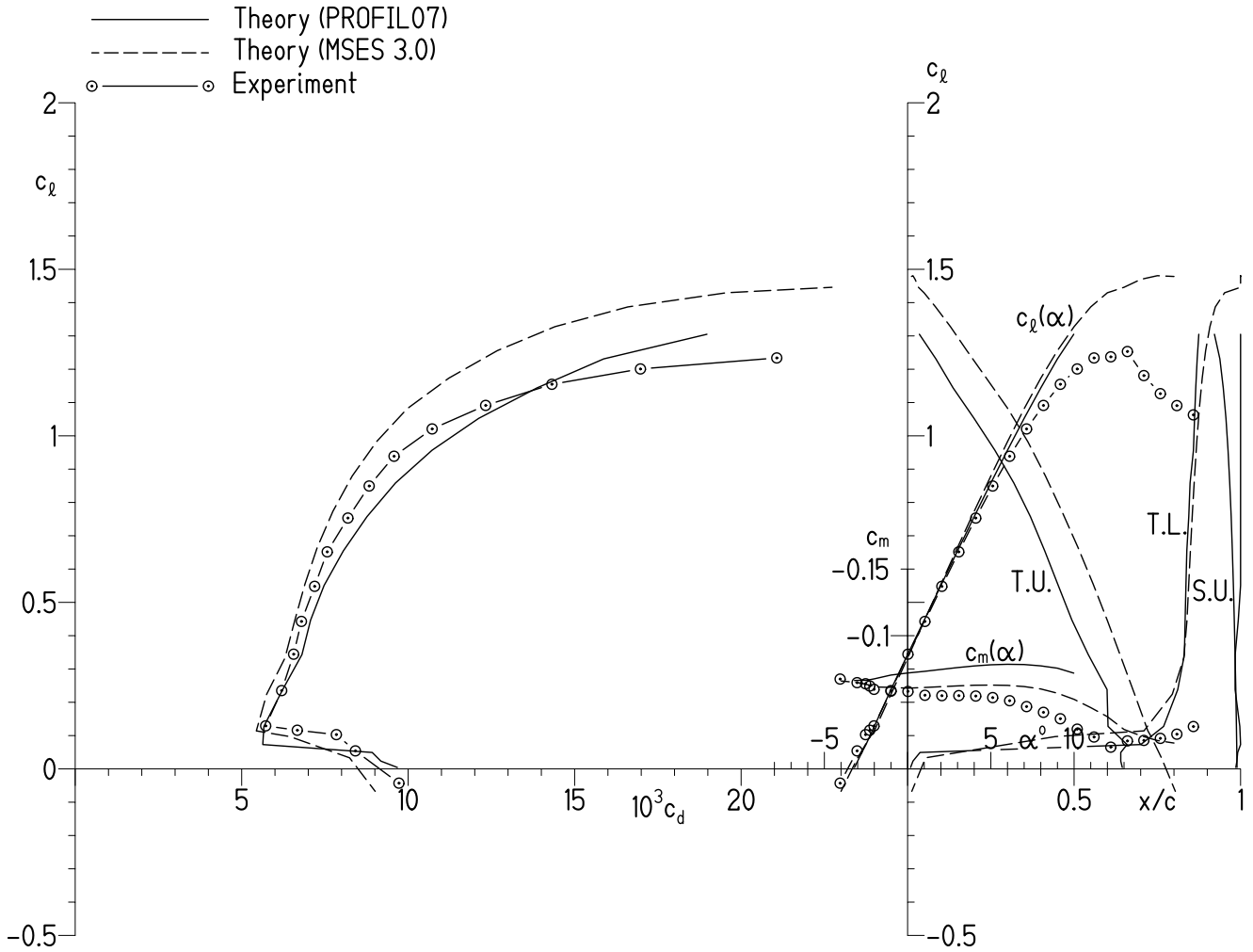

(c) $R = 1.00 \times 10^6$.

Figure 14.- Continued.

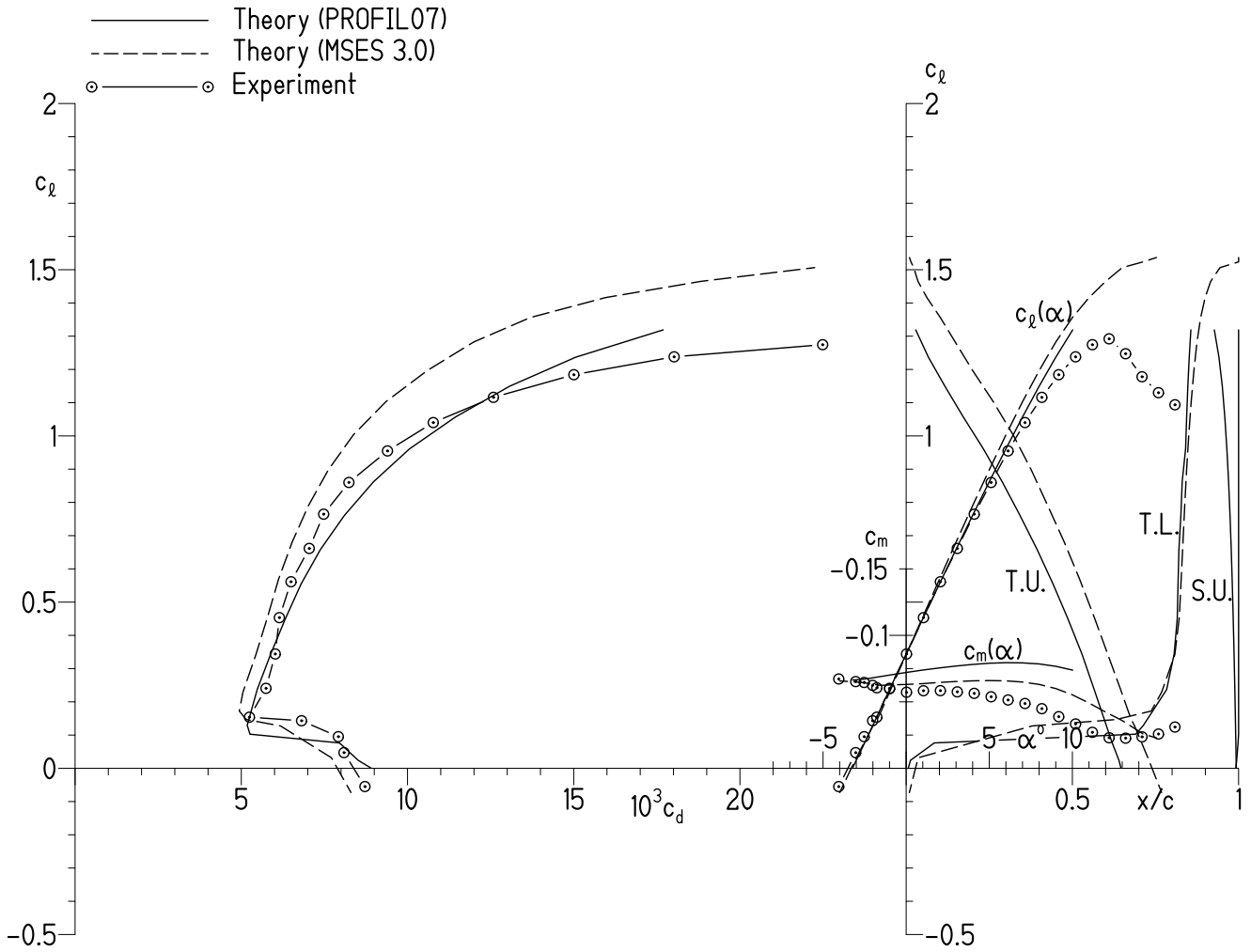

(d) $R = 1.50 \times 10^6$.

Figure 14.- Concluded.

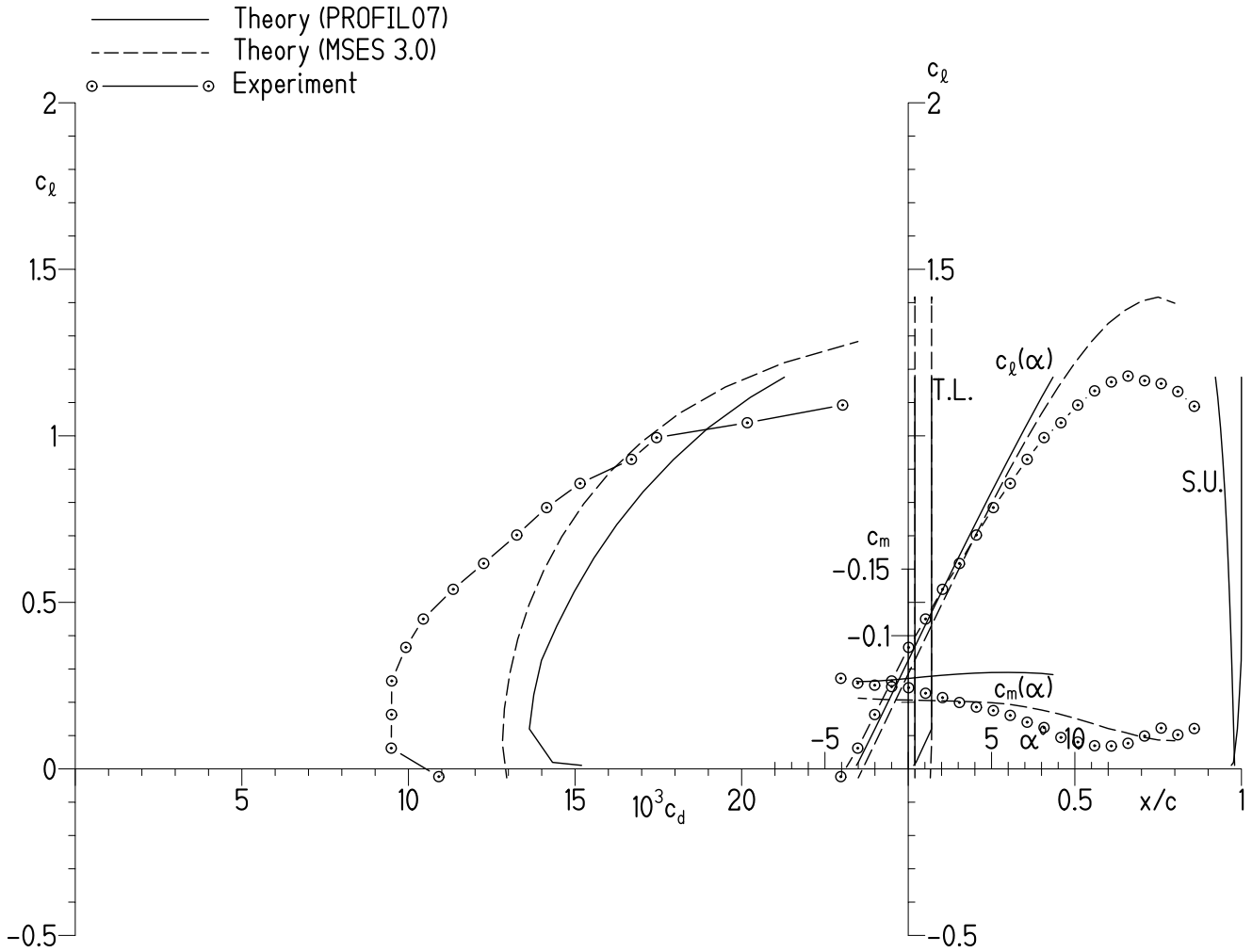

(a) $R = 0.50 \times 10^6$.

Figure 15.- Comparison of theoretical and experimental section characteristics with transition fixed.

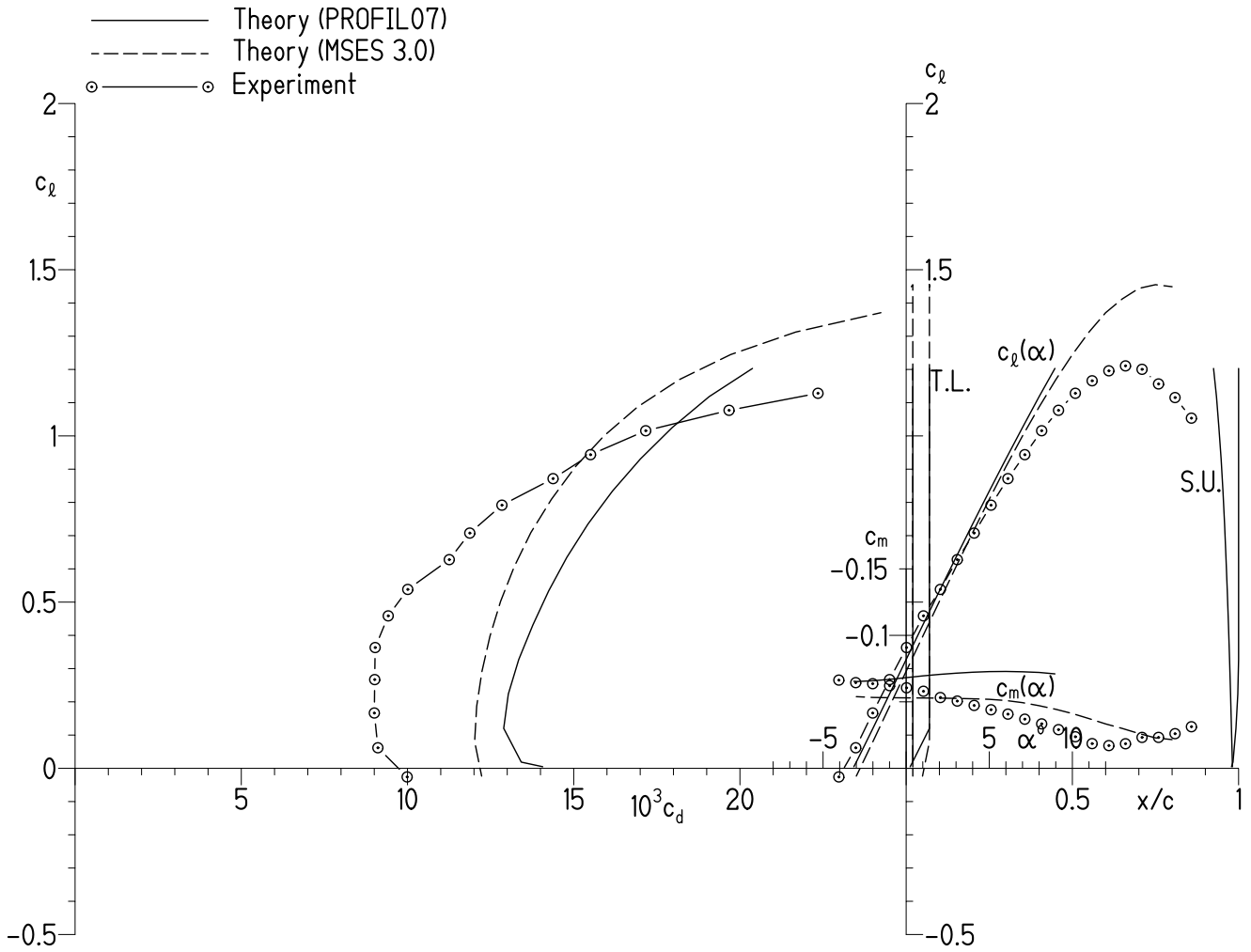

(b) $R = 0.70 \times 10^6$.

Figure 15.- Continued.

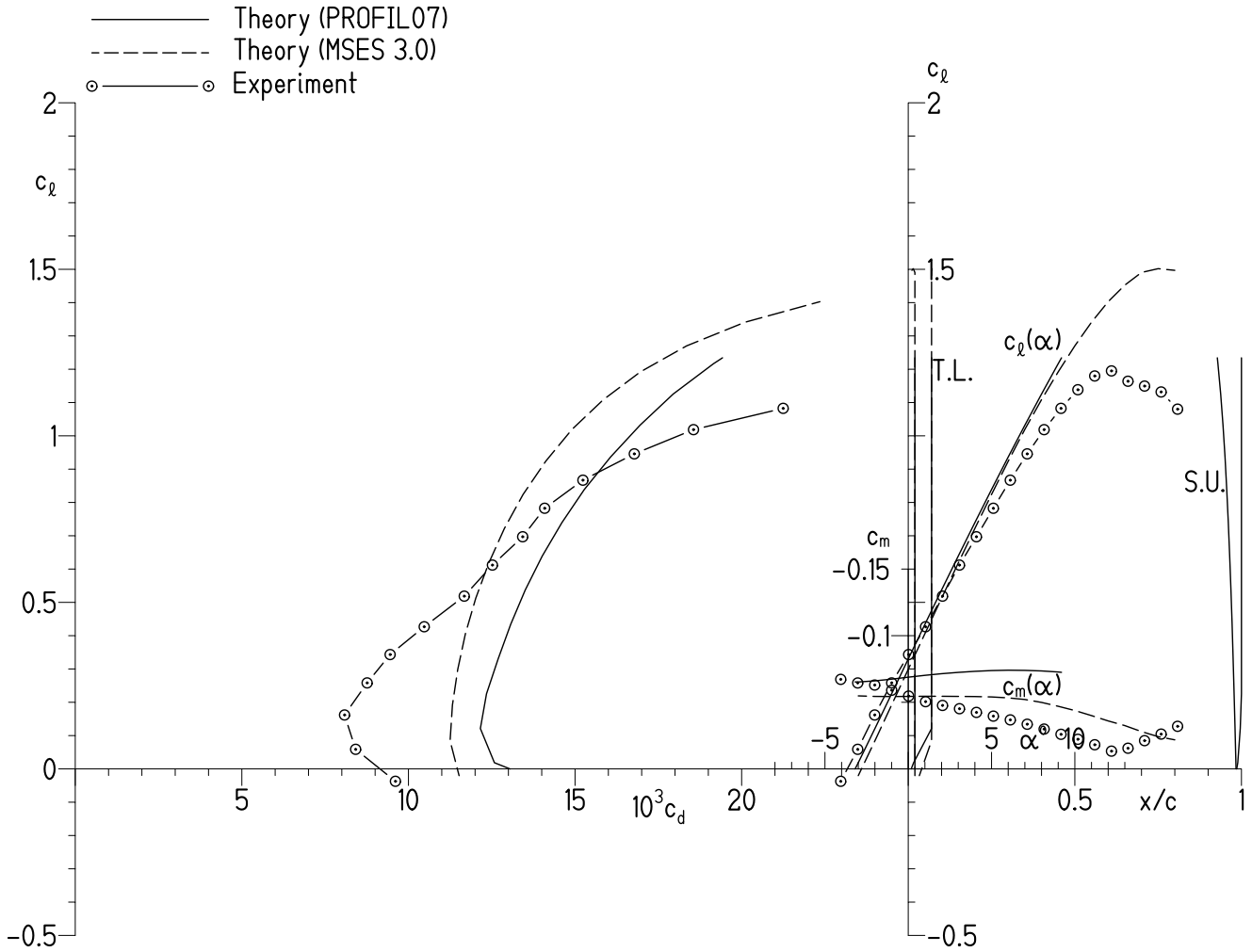

(c) $R = 1.00 \times 10^6$.

Figure 15.- Continued.

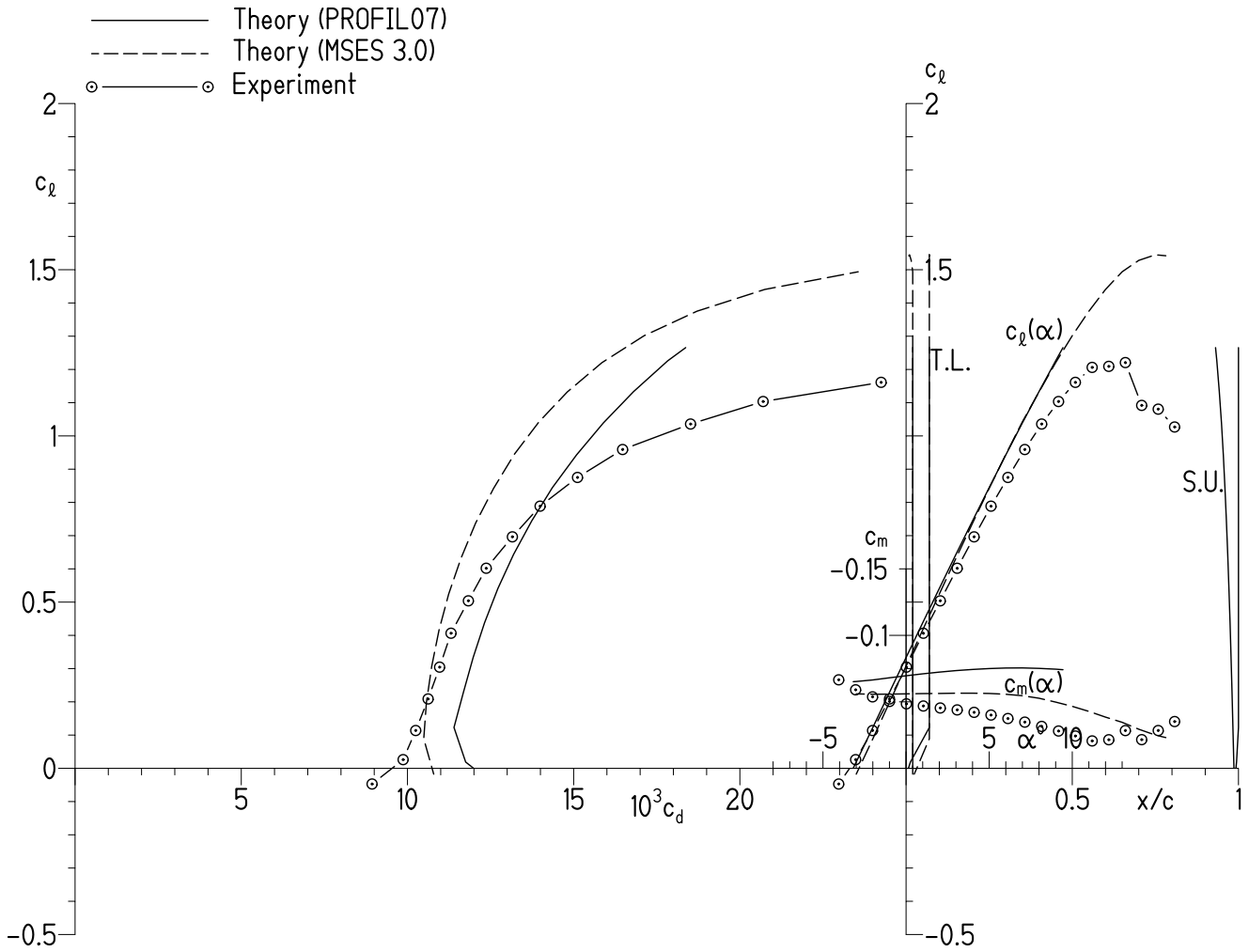

(d) $R = 1.50 \times 10^6$.

Figure 15.- Concluded.

APPENDIX

SECTION CHARACTERISTICS

$R = 0.50 \times 10^6$ and $M = 0.05$ with Transition Free

α, deg	c_l	c_d	c_m
–4.053	–0.0354	0.011075	–0.06872
–3.035	.0507	.009060	–.06401
–2.782	.0625	.007873	–.06255
–2.528	.0762	.007135	–.05983
–2.018	.1279	.007448	–.05801
–.998	.2206	.008663	–.05283
.021	.3193	.008899	–.04943
1.038	.4216	.009032	–.04968
2.055	.5213	.009232	–.04951
3.073	.6220	.009499	–.04887
4.090	.7145	.009974	–.04718
5.107	.8106	.010375	–.04592
6.123	.8986	.011043	–.04440
7.139	.9787	.011835	–.04205
8.154	1.0565	.012971	–.03864
9.168	1.1144	.014523	–.03327
10.179	1.1610	.016671	–.02843
11.191	1.2068	.019790	–.02225
12.198	1.2225	.025501	–.01644
13.201	1.2187	.020191	–.01098
14.197	1.2014	.031392	–.01255
15.191	1.1907	.051522	–.01953
16.178	1.1197	.066080	–.02171
17.164	1.0579	.081776	–.02672

$R = 0.50 \times 10^6$ and $M = 0.05$ with Transition Fixed

α, deg	c_l	c_d	c_m
–4.050	–0.0232	0.010911	–0.06797
–3.033	.0623	.009484	–.06438
–2.015	.1631	.009492	–.06287
–.997	.2640	.009497	–.06173
.021	.3648	.009923	–.06093
1.038	.4500	.010445	–.05680
2.056	.5392	.011342	–.05353
3.071	.6168	.012257	–.04986
4.088	.7022	.013251	–.04644
5.104	.7845	.014147	–.04381
6.119	.8571	.015149	–.04019
7.135	.9294	.016691	–.03508
8.149	.9947	.017447	–.03106
9.162	1.0393	.020168	–.02360
10.173	1.0924	.023030	–.02016
11.183	1.1351	.027513	–.01742
12.187	1.1618	.030099	–.01719
13.189	1.1795	.030230	–.01924
14.183	1.1656	.046598	–.02469
15.178	1.1568	.065548	–.03065
16.178	1.1331	.072738	–.02562
17.167	1.0888	.089178	–.03031

$R = 0.50 \times 10^6$ and $M = 0.05$ Rough

α, deg	c_l	c_d	c_m
–4.052	–0.0280	0.011222	–0.06842
–3.033	.0677	.010347	–.06527
–2.016	.1533	.007926	–.06189
–.998	.2325	.007550	–.05460
.022	.3276	.008682	–.04976
1.039	.4284	.009096	–.04940
2.057	.5299	.008861	–.04924
3.074	.6226	.009825	–.04732
4.091	.7069	.011361	–.04389
5.107	.7846	.012018	–.03981
6.121	.8536	.013582	–.03591
7.136	.9172	.015791	–.03109
8.149	.9756	.018609	–.02658
9.161	1.0265	.023632	–.02199
10.169	1.0557	.035178	–.01738
11.174	1.0687	.050283	–.01500
12.168	1.0592	.097468	–.01949
13.153	.9813	.130726	–.02106
14.141	.9364	.163616	–.02766
15.130	.9004	.196137	–.03408
16.120	.8745	.228290	–.04114

$R = 0.70 \times 10^6$ and $M = 0.07$ with Transition Free

α, deg	c_l	c_d	c_m
–4.052	–0.0313	0.010199	–0.06762
–3.035	.0579	.009036	–.06512
–2.528	.0914	.007172	–.06308
–2.274	.1013	.006370	–.06028
–2.018	.1298	.006800	–.05926
–.999	.2308	.007303	–.05542
.019	.3354	.007602	–.05586
1.037	.4394	.007774	–.05556
2.055	.5402	.008035	–.05449
3.073	.6414	.008485	–.05317
4.091	.7384	.009025	–.05178
5.108	.8348	.009475	–.05099
6.124	.9230	.010352	–.04943
7.141	1.0098	.011474	–.04648
8.157	1.0808	.012620	–.04107
9.170	1.1404	.014536	–.03617
10.183	1.1927	.016573	–.03046
11.194	1.2218	.020362	–.02290
12.201	1.2325	.025432	–.01572
13.201	1.2209	.029810	–.01114
14.197	1.2153	.032923	–.01719
15.186	1.1512	.041441	–.01694
16.175	1.1087	.061829	–.02329
17.159	1.0284	.076866	–.02799

$R = 0.70 \times 10^6$ and $M = 0.07$ with Transition Fixed

α, deg	c_l	c_d	c_m
–4.050	–0.0259	0.009989	–0.06635
–3.034	.0618	.009109	–.06443
–2.015	.1664	.009002	–.06364
–.997	.2669	.009013	–.06215
.021	.3633	.009027	–.06057
1.039	.4586	.009420	–.05797
2.056	.5382	.010008	–.05323
3.073	.6278	.011256	–.05059
4.089	.7077	.011873	–.04731
5.105	.7917	.012840	–.04404
6.121	.8715	.014378	–.04077
7.136	.9436	.015505	–.03696
8.151	1.0156	.017166	–.03344
9.165	1.0771	.019672	–.02909
10.177	1.1283	.022347	–.02374
11.187	1.1659	.028650	–.01859
12.194	1.1959	.037090	–.01710
13.195	1.2107	.028799	–.01848
14.190	1.2004	.059526	–.02327
15.183	1.1564	.054524	–.02328
16.175	1.1154	.071827	–.02607
17.161	1.0535	.086878	–.03129

$R = 0.70 \times 10^6$ and $M = 0.07$ Rough

α, deg	c_l	c_d	c_m
–4.050	–0.0256	0.010351	–0.06638
–3.033	.0703	.009815	–.06548
–2.015	.1626	.009431	–.06252
–.998	.2455	.009210	–.05832
.019	.3153	.009089	–.05129
1.036	.3989	.011085	–.04659
2.053	.4846	.012068	–.04315
3.070	.5667	.012488	–.03908
4.087	.6580	.013550	–.03730
5.103	.7429	.014803	–.03560
6.119	.8249	.016219	–.03291
7.134	.8915	.018491	–.02764
8.147	.9524	.022355	–.02393
9.158	.9982	.030426	–.02012
10.164	1.0168	.048506	–.01621
11.164	1.0203	.076856	–.01795
12.155	.9899	.126975	–.02118
13.143	.9362	.159901	–.02439
14.132	.8968	.192458	–.03066
15.117	.8526	.224645	–.03994
16.107	.8307	.256462	–.04947
17.096	.8064	.287912	–.05855

$R = 1.00 \times 10^6$ and $M = 0.11$ with Transition Free

α, deg	c_l	c_d	c_m
–4.054	–0.0428	0.009723	–0.06745
–3.035	.0541	.008415	–.06475
–2.526	.1029	.007843	–.06393
–2.273	.1161	.006670	–.06224
–2.019	.1292	.005721	–.05974
–1.000	.2351	.006201	–.05838
.019	.3444	.006560	–.05814
1.038	.4428	.006794	–.05530
2.056	.5482	.007191	–.05501
3.074	.6517	.007569	–.05503
4.092	.7532	.008190	–.05470
5.109	.8494	.008829	–.05355
6.126	.9388	.009576	–.05119
7.143	1.0208	.010720	–.04678
8.158	1.0914	.012327	–.04248
9.172	1.1548	.014316	–.03766
10.186	1.2009	.016976	–.02986
11.196	1.2339	.021070	–.02396
12.202	1.2373	.026975	–.01634
13.201	1.2532	.027641	–.02104
14.189	1.1810	.034638	–.02141
15.179	1.1267	.048480	–.02294
16.171	1.0909	.063388	–.02609
17.163	1.0630	.083186	–.03184

$R = 1.00 \times 10^6$ and $M = 0.11$ with Transition Fixed

α, deg	c_l	c_d	c_m
–4.053	–0.0372	0.009609	–0.06722
–3.034	.0588	.008415	–.06452
–2.015	.1619	.008082	–.06296
–.996	.2582	.008760	–.05906
.021	.3433	.009450	–.05467
1.039	.4268	.010473	–.05047
2.056	.5187	.011675	–.04765
3.074	.6120	.012520	–.04519
4.091	.6970	.013428	–.04243
5.107	.7826	.014088	–.03963
6.124	.8669	.015236	–.03680
7.139	.9459	.016778	–.03355
8.154	1.0186	.018555	–.02991
9.168	1.0826	.021246	–.02599
10.181	1.1385	.025341	–.02226
11.191	1.1798	.030733	–.01815
12.197	1.1950	.035860	–.01335
13.189	1.1640	.056752	–.01554
14.183	1.1495	.034823	–.02122
15.178	1.1318	.056535	–.02615
16.165	1.0802	.072582	–.03198

$R = 1.00 \times 10^6$ and $M = 0.11$ Rough

α, deg	c_l	c_d	c_m
–4.054	–0.0803	0.012093	–0.05881
–3.036	.0090	.012189	–.05437
–2.018	.1013	.011980	–.05138
–1.000	.1975	.011892	–.04874
.018	.2929	.012033	–.04673
1.036	.3888	.012225	–.04488
2.054	.4861	.012482	–.04316
3.071	.5776	.012490	–.04143
4.088	.6693	.013229	–.03941
5.104	.7560	.014070	–.03755
6.120	.8355	.015913	–.03363
7.135	.9055	.018444	–.02941
8.148	.9648	.023220	–.02601
9.159	1.0064	.032627	–.02089
10.165	1.0272	.051105	–.01815
11.158	1.0225	.100854	–.02530
12.150	.9789	.134058	–.02575
13.138	.9244	.166891	–.02892
14.125	.8718	.199354	–.03551
15.110	.8266	.231445	–.04507
16.096	.7968	.263164	–.05779

$R = 1.50 \times 10^6$ and $M = 0.17$ with Transition Free

α, deg	c_l	c_d	c_m
–4.056	–0.0549	0.008719	–0.06723
–3.037	.0472	.008089	–.06525
–2.528	.0952	.007919	–.06459
–2.019	.1431	.006813	–.06242
–1.765	.1539	.005245	–.06059
–1.000	.2406	.005743	–.05985
.020	.3440	.006021	–.05725
1.038	.4533	.006145	–.05838
2.057	.5613	.006496	–.05844
3.074	.6615	.007044	–.05753
4.093	.7646	.007477	–.05641
5.111	.8600	.008237	–.05384
6.130	.9549	.009397	–.05144
7.146	1.0402	.010774	–.04877
8.162	1.1161	.012585	–.04489
9.178	1.1842	.015004	–.03888
10.191	1.2380	.018020	–.03340
11.202	1.2745	.022488	–.02710
12.209	1.2921	.033325	–.02302
13.201	1.2473	.025762	–.02272
14.189	1.1781	.039779	–.02372
15.179	1.1301	.053949	–.02582
16.170	1.0938	.073737	–.03108

$R = 1.50 \times 10^6$ and $M = 0.17$ with Transition Fixed

α, deg	c_l	c_d	c_m
–4.054	–0.0472	0.008935	–0.06657
–3.036	.0261	.009869	–.05906
–2.018	.1137	.010248	–.05376
–.999	.2087	.010621	–.05031
.019	.3044	.010967	–.04851
1.038	.4064	.011310	–.04688
2.056	.5039	.011832	–.04539
3.074	.6019	.012369	–.04395
4.091	.6964	.013156	–.04211
5.109	.7887	.013990	–.04008
6.126	.8751	.015115	–.03747
7.142	.9591	.016472	–.03476
8.158	1.0358	.018516	–.03154
9.172	1.1035	.020699	–.02808
10.185	1.1612	.024249	–.02431
11.195	1.2062	.028151	–.02062
12.196	1.2093	.044681	–.02152
13.193	1.2207	.042494	–.02840
14.175	1.0919	.042236	–.02158
15.169	1.0806	.062191	–.02844
16.156	1.0269	.081391	–.03520

$R = 1.49 \times 10^6$ and $M = 0.17$ Rough

α, deg	c_l	c_d	c_m
–4.057	–0.1048	0.012571	–0.05603
–3.038	–.0063	.012085	–.05395
–2.019	.0988	.011620	–.05142
–1.000	.1999	.011537	–.04942
.019	.3007	.011592	–.04742
1.037	.3990	.011992	–.04593
2.056	.4973	.012375	–.04413
3.073	.5907	.013060	–.04209
4.091	.6837	.014023	–.03976
5.108	.7709	.015361	–.03692
6.124	.8528	.017021	–.03388
7.140	.9268	.019846	–.03044
8.153	.9912	.024442	–.02713
9.164	1.0391	.034944	–.02397
10.170	1.0636	.056411	–.02224
11.161	1.0471	.112803	–.03053
12.150	.9880	.145834	–.03115
13.138	.9315	.178490	–.03326
14.123	.8734	.210768	–.03975
15.107	.8235	.242671	–.05106
16.092	.7946	.274198	–.06547

REPORT DOCUMENTATION PAGE

Form Approved
OMB No. 0704-0188

1. REPORT DATE *(DD-MM-YYYY)*	2. REPORT TYPE	3. DATES COVERED *(From - To)*
xx-08-2010	FINAL REPORT	Sep 2007 - Jun 2010

4. TITLE AND SUBTITLE

Design and Experimental Results for the S406 Airfoil

5a. CONTRACT NUMBER
W911W6-07-C-0047

5b. GRANT NUMBER

5c. PROGRAM ELEMENT NUMBER

6. AUTHOR(S)

Somers, Dan M. and Maughmer, Mark D.

5d. PROJECT NUMBER

5e. TASK NUMBER

5f. WORK UNIT NUMBER

7. PERFORMING ORGANIZATION NAME(S) AND ADDRESS(ES)

Airfoils, Incorporated
Attn: Dan M. Somers
122 Rose Drive
Port Matilda PA 16870-7535

8. PERFORMING ORGANIZATION REPORT NUMBER

SBIR Topic Number A06-006
Proposal Number A2-2972

9. SPONSORING / MONITORING AGENCY NAME(S) AND ADDRESS(ES)

US Army Aviation Research, Development and Engineering Command (RDECOM)
Aviation Applied Technology Directorate (AATD)
Fort Eustis VA 23604-5577

10. SPONSOR/MONITOR'S ACRONYM(S)

11. SPONSOR/MONITOR'S REPORT NUMBER(S)
RDECOM TR 10-D-107

12. DISTRIBUTION / AVAILABILITY STATEMENT

Approved for public release; distribution is unlimited.

13. SUPPLEMENTARY NOTES

UL Note: No proprietary / limited information may be included in the abstract.

14. ABSTRACT

A 14.25-percent-thick, natural-laminar-flow airfoil, the S406, for rotorcraft applications has been designed and analyzed theoretically and verified experimentally in The Pennsylvania State University Low-Speed, Low-Turbulence Wind Tunnel. The two primary objectives of high maximum lift and low profile drag have been achieved. The constraint on the airfoil thickness has been satisfied, but the one on the pitching moment has not. The airfoil exhibits a docile stall. Comparisons of the theoretical and experimental results generally show good agreement.

15. SUBJECT TERMS

Airfoils, rotorcraft, laminar flow, wind tunnel

16. SECURITY CLASSIFICATION OF:			17. LIMITATION OF ABSTRACT	18. NUMBER OF PAGES	19a. NAME OF RESPONSIBLE PERSON
a. REPORT	b. ABSTRACT	c. THIS PAGE			Dan M. Somers
unclassified	unclassified	unclassified	UU	66	19b. TELEPHONE NUMBER *(include area code)* (814) 357-0500

Standard Form 298 (Rev. 8-98)
Prescribed by ANSI Std. Z39.18